



Injectable conductive gelatin methacrylate / oxidized dextran hydrogel encapsulating umbilical cord mesenchymal stem cells for myocardial infarction treatment

Shuoji Zhu¹, Changjiang Yu¹, Nanbo Liu¹, Mingyi Zhao¹, Zerui Chen, Jian Liu, Ge Li, Huanlei Huang, Huiming Guo, Tucheng Sun^{****}, Jimei Chen^{***}, Jian Zhuang^{**}, Ping Zhu^{*}

Guangdong Cardiovascular Institute, Guangdong Provincial People's Hospital, Guangdong Academy of Medical Sciences, Guangzhou, 510100, China

ARTICLE INFO

Keywords:

GelMA
Oxidized dextran
Conductivity
Stem cell therapy
Myocardial infarction

ABSTRACT

Umbilical cord mesenchymal stem cells (UCMSCs) transplantation has been proposed as a promising treatment modality for myocardial infarction (MI), but the low retention rate remains a considerable challenge. Injectable natural polymer hydrogels with conductivity ability are highly desirable as cell delivery vehicles to repair infarct myocardium and restore the cardiac function. In this work, we developed a hydrogel system based on gelatin methacrylate (GelMA) and oxidized dextran (ODEX) as cell delivery vehicles for MI. And dopamine could be used as a reductant of graphene oxide (GO) to form reductive GO (rGO). By adjusting the amount of rGO, the conductivity of hydrogels with 0.5 mg/mL rGO concentration ($\approx 10^{-4}$ S/cm) was similar to that of natural heart tissue. *In vitro* cell experiments showed that the prepared hydrogels had excellent biocompatibility and cell delivery ability of UCMSCs. More importantly, GelMA-O5/rGO hydrogel could promote UCMSCs growth and proliferation, improve the myocardial differentiation ability of UCMSCs, and up-regulate the expression of cTnI and Cx43. Further *in vivo* experiments demonstrated that GelMA-O5/rGO/UCMSCs Hydrogel could significantly improve the ejection fraction (EF) of rats and significantly reduce myocardial infarct area compared to PBS group, promote the survival of UCMSCs, enhance the expression level of cTnI and Cx43, and decrease the expression level of caspase-3. The findings of this study suggested that the injectable conductive GelMA-O5/rGO hydrogel encapsulating UCMSCs could improve damaged myocardial tissue and reconstruct myocardial function, which will be a promising therapeutic strategy for cardiac repair.

1. Introduction

Ischemic heart disease is a kind of myocardial ischemic disease caused by coronary artery occlusion [1–3]. Among them, myocardial infarction (MI) with high morbidity and mortality is the most common type, which is seriously harmful to human health [4,5]. The limited ability of cardiac regeneration can lead to scar formation in the infarcted area after MI, resulting in abnormal transmission of electrical signals and asynchronous contraction of the heart [6]. Currently, the existing

treatments can only help to delay but not stop the process of ventricular remodeling [7]. The heart transplantation is the only definitive therapy, but the number of donors is extremely limited by high medical costs and immunosuppressive side effects. Therefore, many researchers try to find suitable biomaterials to replace the lost extracellular matrix (ECM) after MI, and combine stem cell transplantation is an effective way to improve the survival rate of transplanted stem cells in the infarcted area, which will promote exogenous and endogenous myocardial repair [8,9].

Umbilical cord mesenchymal stem cells (UCMSCs) are considered as

; MI, myocardial infarction; UCMSCs, Umbilical cord mesenchymal stem cells; GelMA, Gelatin methacrylate; ODEX, Oxidized dextran; GO, Graphene oxide.

Peer review under responsibility of KeAi Communications Co., Ltd.

* Corresponding author.

** Corresponding author.

*** Corresponding author.

**** Corresponding author.

E-mail addresses: suntucheng@126.com (T. Sun), jimei1965@gmail.com (J. Chen), ZhuangJian2020@hotmail.com (J. Zhuang), tanganqier@163.com (P. Zhu).

¹ These authors contributed equally to this work.

<https://doi.org/10.1016/j.bioactmat.2021.11.011>

Received 10 August 2021; Received in revised form 4 November 2021; Accepted 7 November 2021

Available online 17 November 2021

2452-199X/© 2021 The Authors. Publishing services by Elsevier B.V. on behalf of KeAi Communications Co. Ltd. This is an open access article under the CC

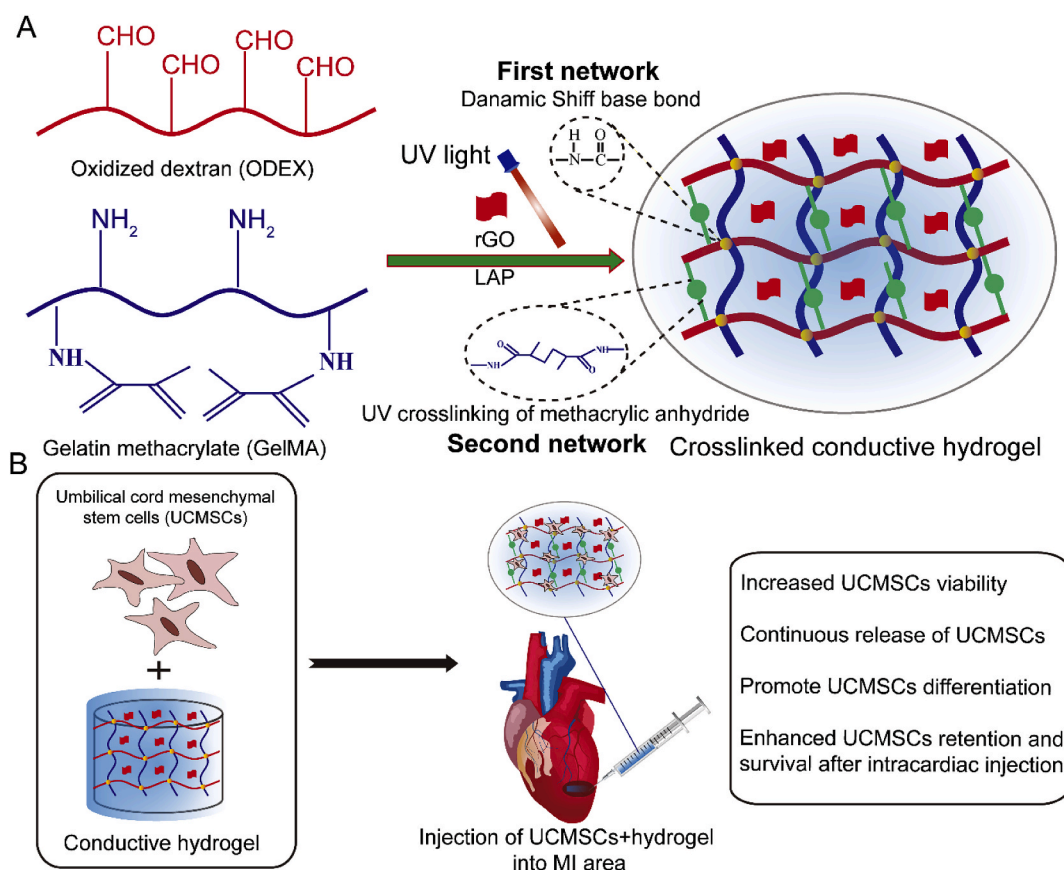
BY-NC-ND license (<http://creativecommons.org/licenses/by-nc-nd/4.0/>).

a new type of seed cells for heart tissue engineering because of their potential to differentiate into myocardium via paracrine action [10]. However, tissue regeneration using stem cell transplantation faces many obstacles, such as low cell retention rate, low survival rate and incomplete differentiation following transplantation. Injectable hydrogel can quickly complete the phase transition and maintain a three-dimensional structure similar to extracellular matrix after becoming solid, which could be applied to stem cell transplantation and growth factor carriers in MI [11–13]. Previous studies have shown that folic acid derived hydrogel can improve the survival time of induced pluripotent stem cell (iPS) transplantation and significantly improve the myocardial differentiation efficiency of iPS *in vivo* [14]. Many researchers applied injected natural hydrogels (alginate [15], dextran [16], gelatin [17], hyaluronic acid [18] and extracellular matrix derivatives [19]) with low irritation, good cell affinity and excellent properties into the infarcted area, which could significantly improve left ventricle function, decrease infarct size and wall thickness within the infarct region, thus improving cardiac function. GelMA hydrogel has been used to regulate the delivery of growth factors and stem cells in various tissue engineering applications, especially in the field of skin tissue and cartilage tissue regeneration [20]. In addition, previous studies have shown that GelMA hydrogel is expected to be used as a stem cell delivery carrier for myocardial tissue regeneration [21]. However, pure GelMA hydrogel present poor mechanical properties and rapid degradation [22]. Therefore, we added oxidized dextran (ODEX) to form interpenetrating polymer network (IPN), to enhance external energy dissipation and reduce the degradation rate of hydrogels.

Myocardial tissue also conducts electrophysiological signals in the process of continuous contraction and relaxation, so hydrogel with conductivity has become the major research projects [23,24]. Previous studies have demonstrated the role of conductive biomaterials in the

process of myocardial repair [25,26]. Graphene is a promising candidate material because of its excellent electrical conductivity, biocompatibility. However, the poor dispersion of graphene seriously limits the application of graphene. Graphene oxide (GO) shows better water dispersibility because of its hydrophilic groups, such as hydroxyl, epoxy and carboxyl groups [27]. However, compared with graphene, its electrical conductivity is much lower. Fortunately, under the condition of weakly alkaline pH, dopamine can be used as a reductant of GO to form reductive GO (rGO), to improve its electrical conductivity. In addition, the obtained rGO not only has good dispersion, but also has good conductivity. Previous studies reported rGO-GelMA hydrogels as scaffolds exhibit excellent cell viability, proliferation, and maturation for Cardiomyocytes [28]. Furthermore, we combined rGO with UCMSCs to prepare the bioactive conductive hydrogels, which will considerably enriched the application field of intelligent conductive hydrogels.

In this study, we aim to develop an injectable conductive hydrogel based on rGO and GelMA/ODEX matrix as cell delivery carriers of UCMSCs to promote MI repair (Scheme 1A). Firstly, gelatin methacrylate (GelMA) and oxidized dextran (ODEX) were synthesized and characterized, and then mixed with different concentration of rGO and photoinitiator (LAP), GelMA-O5/rGO conductive hydrogel was prepared under ultraviolet (UV) light condition. The three-dimensional structure, swelling properties, rheological properties, compressibility and degradability of these hydrogels were characterized. Four-probe tester was used to characterize the electrical properties of the composite hydrogel system. In addition, the cytocompatibility ability of cell encapsulation and cell differentiation in hydrogels were studied in detail. The results indicated that GelMA-O5/rGO conductive hydrogel could provide a three-dimensional microenvironment for cell growth *in vitro*, promote stem cells to differentiate into myocardium, and improve damaged myocardial tissue and reconstruct myocardial function *in vivo*



Scheme 1. (A) Synthesis route of conductive GelMA-O5/rGO hydrogel. (B) Conductive GelMA-O5/rGO hydrogel system encapsulating UCMSCs for cardiac repair by injection into the MI area.

(Scheme 1B). In summary, all of these results demonstrate that the conductive hydrogel is expected to be used as the carrier of UCMSCs encapsulation and differentiation, and has great potential in the repair of MI.

2. Experimental section

2.1. Materials and reagents

Gelatin (type A, from porcine skin), methacrylic anhydride (MA), and sodium periodate (NaIO_4) were obtained from Aladdin Industrial Corporation (Shanghai, China). Dextran ($M_w = 70$ kDa) was purchased from J&K Scientific co., Ltd (Beijing, China). Lysozyme was purchased from commercially Shanghai Yuanye Bio-Technology Co., Ltd. (Shanghai, China). Human umbilical cord mesenchymal stem cells (UCMSCs, AC340316) was purchased from American Type Culture Collection (Manassas, VA). Live/Dead cell staining kits, Cell Counting Kit-8 (CCK-8), Calcein-AM, propidium iodide, 4,6-diamidino-2-phenylindole (DAPI) and TRITC Phalloidin were purchased from Biyuntian Biotechnology CO. LTD. (Shanghai, China). All of the chemical reagents were of analytical grade and used without any further purification.

2.2. Synthesis of GelMA and ODEX

GelMA was synthesized as described previously [29]. First, 10 g of gelatin was added to 100 mL of PBS at 50 °C, and the solution was stirred until the gelatin had dissolved. Then, 6 mL of MA was added dropwise into the gelatin solution, and the solution was stirred for 1 h until it became milk white. Finally, the mixed solution was dialyzed against deionized water using dialysis bag ($MWCO = 3500$ Da) and placed in deionized water at 40 °C for 1 week to obtain GelMA polymer. Samples were lyophilized and stored at –20 °C until further use. ODEX was synthesized according to the reported procedure [30]. First, 5 g of DEX was added to 250 mL deionized water at a concentration of 2% (w/v), and the solution was stirred until the DEX had dissolved. Then, 5.0 g of sodium periodate was added to the above solution while protected from light, and after reacting for 3.5 h, 3 mL of ethylene glycol was added to quench the unreacted sodium periodate. Finally, the mixed solution was dialyzed against deionized water using dialysis bag ($MWCO = 8000$ – 14000 Da) for 3 days against deionized water to obtain ODEX polymer. Samples were lyophilized and stored at 4 °C until further use. The oxidation percentage of dextran was 52.6%, which was determined by quantifying the concentration of periodate left unconsumed using iodometry after 3.5 h. Briefly, 5 mL of reaction mixture was neutralized with 10 mL 10% (w/v) sodium bicarbonate solution. Then 2 mL of 20% (w/v) potassium iodide solution was added and incubated for 15 min at room temperature in the dark. Finally, the iodine was titrated with 0.1 mol/L of sodium thiosulphate ($\text{Na}_2\text{S}_2\text{O}_3$) solution using starch as an indicator [35].

2.3. Preparation of composite hydrogel

2.3.1. Preparation of the hydrogels

The freeze-dried GelMA and ODEX were dissolved in PBS at 60 °C to make the final GelMA concentrations at 50 mg/mL with different ODEX concentrations of 0, 50 and 70 mg/mL, named GelMA, GelMA-O5 and GelMA-O7 hydrogels, respectively. Subsequently, 0.1% (w/v) photoinitiator LAP was added, and the prepolymer solution incubated at 37 °C for 15 min to form the Schiff's bases, and then exposed exposure to 30 mW/cm² blue light (405 nm) for 20 s.

2.3.2. Synthesis of dopamine reduced GO (rGO)

rGO was synthesized by stirring GO and dopamine hydrochloride under alkaline conditions (Tris-HCl buffer). Briefly, dopamine hydrochloride (10 mg) and GO (10 mg) were dissolved in 20 mL Tris-HCl buffer (0.05 M, pH = 8.5) and sonicated for 30 min. After 24 h

stirring at room temperature, the resulting mixture was purified and separated by filtration and further washed with water and ethanol several times to obtain the rGO composite. Finally, the rGO was dried at 60 °C under high vacuum conditions for 48 h. The morphology of GO and rGO were characterized using transmission electron microscopy (JEOL JEM-1210, JEOL Ltd, Tokyo, Japan). The particle size of GO and rGO were measured with a Nano-ZS instrument (Nano-ZS; Malvern Instruments, UK). The X-ray diffraction patterns of GO and rGO were measured with an X-ray powder diffractometer (XRD, Gemini S Ultra) with an angle between 5 and 75°.

2.3.3. Preparation of conducting hydrogel

First, rGO was dispersed in PBS at room temperature with different concentrations of 0.1 wt%, 0.5 wt% and 1.0 wt%, respectively. 0.5 mL of above rGO dispersion or 0.5 mL of DI water was added into 4 mL of GelMA-O5 solution to prepare the mixed solutions. The synthesis of the GelMA-O5/rGO hydrogel was also in accordance with the above procedure.

2.4. Characterization

2.4.1. FT-IR, SEM and ¹H NMR test

The Fourier transform infrared spectroscopy (FTIR) spectra of DEX, ODEX were recorded with FTIR spectroscopy (Spectrum One, PerkinElmer, Norwalk, USA) to confirm the expected pendant functionalities. For each spectrum, 64 scans at a resolution of 4 cm⁻¹ were obtained. The morphology of hydrogels was observed using a scanning electron microscope (SEM; S-3400, Hitachi, Japan), and the pore size of the hydrogel was measured using IPP6.0 software. The chemical structure of gelatin, Gel and GelMA was performed by ¹H NMR (AVANCE III 600 M, Bruker, Germany). The degree of methacrylation was calculated according to the following equation:

$$\text{Degree of methacrylation (DM)} = \frac{I_{5.27}}{I_{5.27} + I_{2.84}} \times 100\%$$

2.4.2. Swelling ratio measure

The swelling capacity of hydrogels was determined using the gravimetric change. Briefly, Test hydrogels were weighed (W_0) and then immersed in PBS. At a predetermined time, the hydrogels were removed from the PBS and wiped off with filter papers, and the swollen weight (W_t) was recorded. The swelling ratio was calculated according to the following equation:

$$\text{Swelling ratio (\%)} = (W_t - W_0) / W_0$$

2.4.3. Rheological test

Dynamic rheological tests of the hydrogels were tested by a TA rheometer instrument (Kinexus, Ma Erwen instruments, Britain). All hydrogel samples were prepared as discs 8 mm in diameter and 2 mm in height. Time-sweep oscillatory tests of the hydrogels ($n = 3$) were performed at a 1% strain, 1 Hz frequency and a 0.5 mm gap (CD mode) for 600 s. Frequency-sweep experiment was performed at shear rates ranging from 0.1 to 100 rad/s.

2.4.4. Compression test

The compressive stress–strain measurements were performed on hydrogel samples via an universal testing machine (model 5543; Instron, Norwood, MA). In compression-crack test, hydrogel samples were shaped into cylinders of 12 mm in diameter and 8 mm in high. A strain rate (compression) of 1 mm min⁻¹ was employed and strain level was up to ≈60%. The compressive modulus at 60% stress was defined as compressive modulus.

2.4.5. In vitro degradation rate of the hydrogel

The degradation tests of the hydrogel were carried out according to

previous literature [10]. The biodegradability of hydrogels was determined by weighing the samples at different time points. The GelMA, GelMA-O5, GelMA-O5/rGO (rGO = 0.5 mg/mL) hydrogels were then immersed in 20 mL PBS (pH = 7.4) containing either 0 or 1000 U/mL lysozyme at 37 °C with a stirring rate of 50 rpm for 2 weeks. At each time point, the degraded samples were washed with PBS, and lyophilized and weighted. The weight loss rate of hydrogel was calculated using the formula:

$$\text{Weight loss rate} = W_t/W_0 \times 100\%$$

Where W_0 is the initial mass of the lyophilized hydrogel, and W_t is the final mass of the lyophilized hydrogel at each time point.

2.5. Conductivity measurement

The GelMA-O5 hydrogels solutions with different rGO concentration was absorbed by a syringe and dripped into a transparent sheet mold with a spacing of 0.5 mm, and the flake hydrogel sample was formed after UV irradiation. The conductivities of the hydrogels were tested using a four-point probe (Jandel RM3, Leighton Buzzard, UK).

2.6. Biocompatibility test in vitro

UCMSCs were cultured in Dulbeccos modified Eagle medium F12 (DMEM/F12) supplemented with 10% fetal bovine serum (FBS), 1% penicillin/streptomycin in 5% CO₂ at 37 °C. Cells at passage 3–5 were used in the following experiments. Test GelMA-O5 and GelMA-O5/rGO (rGO = 0.5 mg/mL) hydrogels (500 µL) were added on the 12-well plate with a pipette gun. After induced by blue light (405 nm) for 20 s, 2 mL cell suspension of UCMSCs (2×10^4 cells/mL) was added onto the hydrogel surface and cultured in DMEM supplemented with 10% FBS, 2% L-glutamine and 1% antibiotic under 37 °C, 5% CO₂ conditions. The culture medium was changed every two days. Subsequently, culture the cells for different time (1, 3, and 5 days) at 37 °C under the humidified atmosphere containing 5% CO₂. Live and dead cells after culture on the hydrogels were visualized by using the Live/Dead staining kit according to manufacturer's instructions. The cell attached-hydrogels in each well were rinsed with PBS for three times, and then added 2 mL of a live/dead reagent (Calcein-AM/PI). After incubation at 37 °C for 20 min, photos of the stained samples were observed by a confocal laser microscope (FV 3000, Olympus, Japan). Meanwhile, test hydrogels were fixed and counterstained by the F-actin with TRITC Phalloidin and nuclei with 4, 6-diamidino-2-phenylindole (DAPI). The hydrogels were observed by a confocal laser microscope. In addition, the cell viability on hydrogel was quantitatively analyzed by CCK-8 assay. At the time points indicated, the culture medium was replaced with 2 mL serum-free culture medium containing 40 µL CCK-8 solution. After incubation 2 h at 37 °C, the absorbance at 450 nm of the solutions was measured in 96-well plates using a microplate reader (Molecular Devices, Sunnyvale, CA).

2.7. Cell encapsulation and cell release study

2.7.1. Cell encapsulation in the hydrogel

Cell encapsulation was conducted following previously published protocols [31]. Firstly, GelMA-O5 and GelMA-O5/rGO (rGO = 0.5 mg/mL) hydrogels (500 µL) contained UCMSCs (1×10^7 cells/mL) were added on the 12-well plate with a pipette gun. After induced by blue light (405 nm) for 20 s, 2 mL fresh cell culture growth medium was added to each well and hydrogels encapsulated cells were cultured in a humidified atmosphere at 37 °C containing 5% CO₂. After being cultured for 1, 3 and 5 days, the cell number in the hydrogel were counted by the CCK-8 assay and photos of the stained samples were observed by a confocal laser microscope (FV 3000, Olympus, Japan).

2.7.2. In vitro cell delivery property of the hydrogel

To investigate the encapsulated UCMSCs release in the hydrogel, the encapsulated cells were prepared following the same protocol above described. After being cultured for 1–6 days, we transferred DMEM from each well to a new well and then added 2 mL fresh DMEM into the hydrogel's well. The viability and proliferation of released cells in transferred cell culture growth medium was determined using the Live/Dead staining kit and the automatic cell counter (Countess II FL, Thermo-fisher, USA). After being cultured on the 12-well plate for 2 days, the released cells were observed by an optical microscope (TE2000-S, Nikon, Japan).

2.8. Cardiac differentiation of UCMSCs

After cultivation under differentiation media in petridish (Thermo-fisher brand) for 7 days, the UCMSCs in the tissue culture plates (TCPs), GelMA-O5 and GelMA-O5/rGO hydrogels were fixed in 4% cold paraformaldehyde aqueous solution at room temperature for 10 min. The culture medium was changed every three days. After being rinsed for three times with PBS, the gels placed overnight in a 30% (w/v) sucrose in PBS solution at 4 °C. The gels were frozen at –20 °C and cut into sections with a thickness of 20 µm. After blocking with 1% bovine serum albumin (BSA)/PBS at room temperature for 30 min, the samples were incubated with the primary antibody rabbit anti-cardiac troponin I (cTnI, ab47003, abcam, 1: 100) and rabbit anti-connexin 43 (Cx43, ab11370, abcam, 1: 100) in 1% BSA overnight at 4 °C. After being washed with PBS for several times, the samples were incubated with an Alexa Fluor488 Donkey anti-rabbit IgG (H&L) secondary antibody (A11034; Invitrogen, 1: 500) for cTnI detection in PBS for 1 h. After being rinsed with PBS, further stained with DAPI and then imaged using the confocal laser microscope (Olympus FV1000, Tokyo, Japan).

2.9. Western blot analysis

After cultivation for 7 days, the UCMSCs in the tissue culture plates (TCPs), GelMA-O5 and GelMA-O5/rGO hydrogels were washed with PBS. Then the cells on the gels were treated with liquid nitrogen and smashed. The protein samples were extracted using radio-immunoprecipitation assay (RIPA) protein extraction solution supplemented with protease on the ice for 30 min. The extracted proteins were determined by BCA protein assay (Beyotime, Jiangsu, China). The proteins (20 µg/lane) were resolved by 12% sodium dodecyl sulfate (SDS)-polyacrylamide gels and then the separated proteins were transferred to polyvinylidenedifluoride (PVDF) membranes (0.45 mm; Millipore, Bedford, MA). After blocking with 5% milk for 2 h at room temperature, the membranes were incubated antibodies against rabbit anti-cTnI (ab47003, abcam, 1: 100) and rabbit anti-Cx43 (ab11370, abcam, 1: 100) overnight at 4 °C. After being rinsed for three times with Tris buffered solution (TBST), the membrane was incubated in goat anti-rabbit secondary antibodies conjugated with horseradish peroxidase (HRP) for 1 h at room temperature. Densitometric analysis was determined using Image J analysis software and β-actin was used as an internal standard.

2.10. Quantitative real-time polymerase chain reaction (qRT-PCR)

After cultivation for 7 days, total RNAs of the UCMSCs in the sample was performed using the Prime Script™ RT reagent Kit with gDNA Eraser (Takara) as per manufacturer's instructions. Three biological replicates of each sample were collected. And analysis of expression was performed by the SYBR green system (Qiagen). Amplifications for cDNA samples were carried out at 30 s at 95 °C, followed by 40 cycles (95 °C for 30 s, 60 °C for 30 s and 72 °C for 20s). Primers for cTnI and Cx43 are summarized in Table S1 and β-actin was used as the housekeeping gene. Relative gene expression of target genes was quantified relative to β-actin, a housekeeping gene, and calculated using the $2^{-\Delta\Delta Ct}$ (Livak

method). All experiments were performed at least in triplicate.

2.11. Establishment of MI model

All animal experimental protocols have been reviewed and approved by the Animal Protection and Use Committee of Jinan University. Animals were divided into 5 groups ($n = 10$ for each group) as follows: sham operation, MI only PBS as the control group, GelMA-O5 hydrogel group, GelMA-O5/rGO hydrogel group, GelMA-O5/rGO/UCMSCs (1×10^6 UCMSCs) hydrogel group.

Sprague Dawleymale rats, 6 weeks of age, were used in this study. Rats were anesthetized with 3% sodium pentobarbital (60 mg/kg of body weight). A left hemi-thoracotomy was performed to enable visualization of the heart, and MI was produced by permanent ligation of the left anterior descending artery (LAD) using a 7–0 prolene suture. The lungs were re-expanded, and the color changes in the ischemic portion of the myocardium could be observed. Next, a volume of 50 μ l of each hydrogel was administered by multipoint injection into the border of the infarction using a 26 gauge needle, and was then irradiated by blue light (405 nm) for 20 s. After the surgery, the chest was closed with a 6-0 silk suture, and the muscle and skin were then closed with a 4-0 silk suture. Cefazolin sodium (a dose of 5%) was administrated intramuscularly on the 2 consecutive days after the surgery to prevent infection and minimize swelling at the surgery site. At days 7, 14 and 21 post-injection, right and left ventricular function were assessed using a Millar catheter (Millar Instruments, Houston, TX). Four weeks after the injection, all animals were sacrificed after functional analysis, and the hearts were collected for further histological analysis.

2.12. In vivo cell tracer experiment

To investigate the location of the transplanted UCMSCs and their fate in the infarcted area, the red fluorescent dye PKH26 was used to label UCMSCs according to the manufacturer's instructions. The MI Rats ($n = 4$ /group) received intramyocardial injections of either 50 μ l of DMEM containing 1×10^6 UCMSCs or GelMA-O5/rGO hydrogel containing 1×10^6 UCMSCs. The PKH26 labeled cells in the heart tissues were captured with inverted fluorescence microscope at days 1, 3 and 7.

2.13. Histological analysis

Heart tissue samples were routinely fixed with 4% paraformaldehyde overnight and embedded in paraffin. The embedded tissues were serially sectioned at 3 μ m using the microtome (Leica Biosystem, Vienna, Austria). To evaluate myocardium fibrosis after MI, heart tissues were stained with Masson's trichrome according to the manufacturer's instructions. The fibrosis area and left ventricular (LV) wall thickness quantified using the IPP 6.0 software in the same section ($n = 10$). The LV wall thickness was calculated through measuring values of the infarcted left ventricular wall thickness. The fibrosis area was calculated according to the following equation:

$$\text{Fibrosis area (\%)} = (\text{fibrous tissue area} / \text{entire heart tissue}) \times 100$$

2.14. Immunofluorescence staining analysis

For immunofluorescence staining, tissue sections were incubated with primary antibodies including anti-cTnI (ab47003, abcam, 1: 100) and anti-Cx43 (ab11370, abcam, 1: 100) and anti-Caspase-3 (ab179517, abcam, 1: 100) overnight at 4 °C. After rinsed the slices with PBS, tissue sections were then stained with the HRP-conjugated goat anti-rabbit secondary antibodies (A11034; Invitrogen, 1: 500). To visualize nuclei cells were counterstained with DAPI. The fluorescence images were captured using an inverted fluorescence microscope (TE2000-S, Nikon, Japan), and positive areas were analyzed by Image Pro-Plus 6.0

software.

2.15. Statistical analysis

All experiments were replicated at least three times and displayed as means \pm standard deviation (SD). Data were tested for normal distribution and significant differences were determined by one-way analysis of variance (ANOVA) analysis with post hoc tests. A value of $p < 0.05$ was considered to be statistically significant (* $p < 0.05$, ** $p < 0.01$, *** $p < 0.001$). All experiments were performed at least three times and presented as means \pm standard deviation (SD).

3. Results and discussion

3.1. Characterization of the hydrogel

In order to form hydrogels for myocardial repair, ODEX was synthesized by oxidizing dextran with sodium periodate and GelMA polymers were synthesized by the reaction of MA with gelatin. The synthetic route of ODEX and GelMA is shown in Fig. 1A and Fig. 1B, respectively. The FTIR spectrum of DEX and ODEX showed that the slightly presented absorption peaks of the aldehyde group coupled with 1722 cm^{-1} indicated the ODEX (Fig. 1C). The ^1H NMR spectrum of GelMA had two peaks at 5.27 ppm and 5.51 ppm (Fig. 1D), indicating that the methacrylic group was successfully grafted onto the molecular backbone of gelatin. These data demonstrated the successful synthesis of ODEX and GelMA polymer. The degree of substitution with the methacrylate group used in this study was 56.8% yield using ^1H NMR spectroscopy (Fig. S1). The TEM images showed that both GO and rGO are lamellar, and rGO achieved good dispersion than GO (Fig. S2A). As shown in Fig. S2B, the XRD spectra showed the GO characteristic peak at 10.92°, which corresponds to an interlayer spacing of 0.81 nm [32]. However, there was no peak at 10.92° in the XRD spectra of rGO, which was due to that a thin layer of PDA occupy the GO surfaces, preventing GO stacking and aggregation [33]. Meanwhile, the average size of rGO was significantly reduced (190.1 ± 6.7 nm) from those of pristine GO (458.7 ± 7.3 nm) (Figs. S2C and S2D).

As shown in Fig. 2A, a primary cross-linking network is formed by the Schiff reaction between ODEX and GelMA. A second cross-linking network of hydrogel polymerization (the C=C bonds will undergo free radical polymerization) was then formed by exposing the hydrogel to blue light for 20 s [34]. The GelMA-O5 hydrogels can be conveniently injected into the PBS solution at room temperature under a 405 nm blue light through a syringe and maintain their shape without any liquid leakage (Supplementary Video 1). The hydrogel morphology displayed enormous porous structure both on the surface and in the inner structure (Fig. 2B). This pore structure was contribute to exchange a large amount of water and nutrients, and it may serve as a supporting wall at the peri-infarct site. The calculated pore size for GelMA, GelMA-O7, GelMA-O5 hydrogels were 43.47 ± 15.46 μ m, 54.93 ± 19.68 μ m, and 54.01 ± 19.98 μ m, respectively (Fig. S3). And there was no significant difference. As shown in Fig. 2C, The GelMA hydrogel is stable in PBS and the swelling ratio is $33.25 \pm 2.36\%$. The addition of ODEX and rGO slightly reduced the swelling rate of the hydrogel, which may be due to higher cross-linking density. All groups showed a stable inflation rate within the range of 24–33%.

3.2. Compression modulus and rheological properties

An ideal hydrogel for myocardial repair should equip with good mechanical properties to keep its integrity during use. As shown in Fig. 2D, the GelMA-O5/rGO hydrogel had a higher modulus (>200 kPa), which reached within the range of the native myocardium modulus (≈ 101 – 102 kPa) in the physiological strain regime [35]. Compared with pure GelMA groups, the compression modulus of GelMA-O5 increased significantly, which might due to more compact structure in GelMA-O5

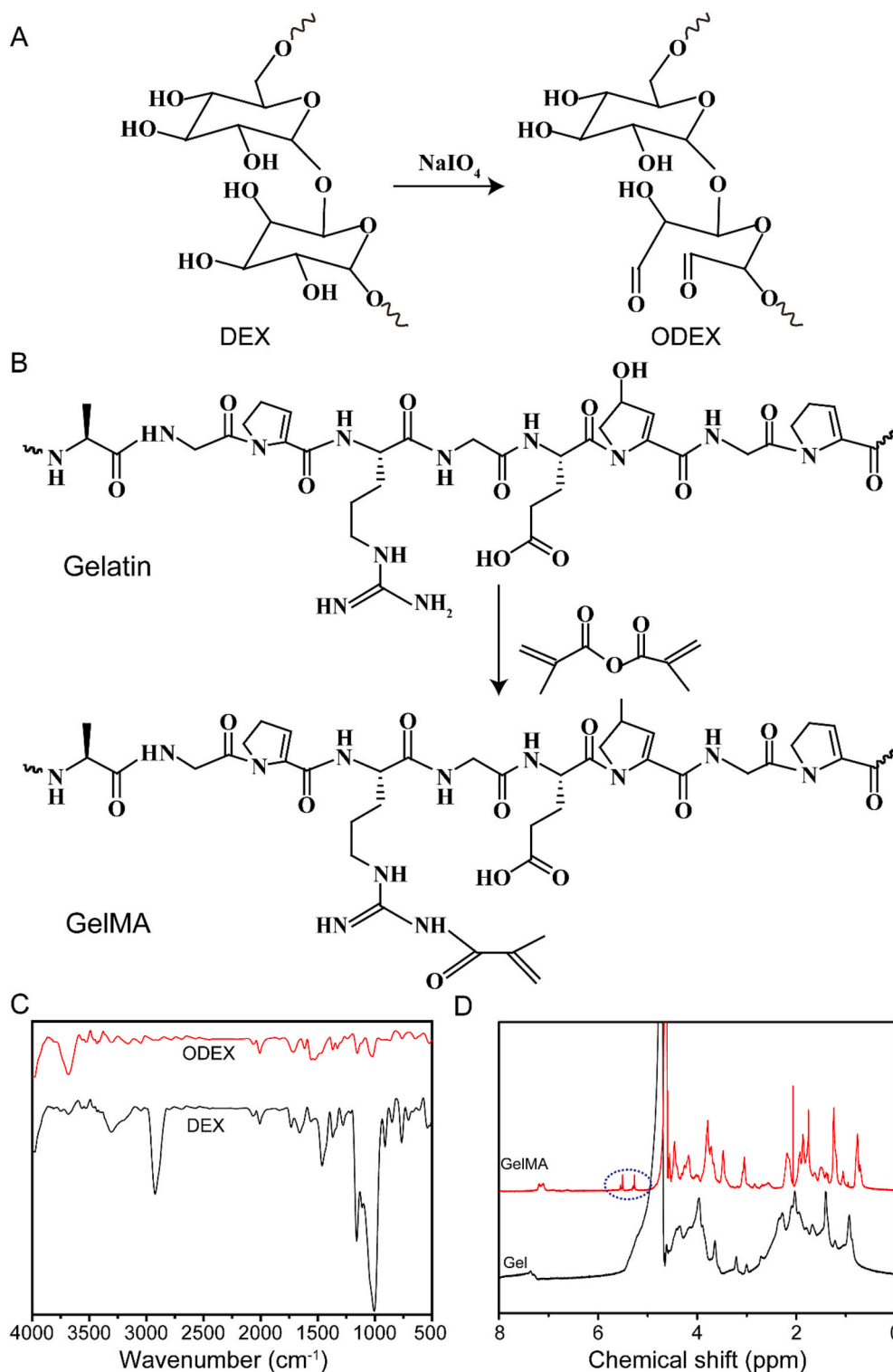


Fig. 1. (A) The synthesis steps of ODEX. (B) The synthesis steps of GelMA. (C) FTIR spectra of DEX and ODEX. (D) ^1H NMR spectra of Gel and GelMA.

hydrogel. Although the rGO incorporated GelMA-O5 hydrogel shown slightly increased compression modulus (~ 13.7 kPa), the differences were not statistically significant. The slightly increased compression modulus was mainly due to the high Young's modulus and highly flexible macromolecular sheet structure of the GO nanosheets, and a very low concentration of rGO in GelMA-O5 hydrogel. Cyclic compression testing was tested to evaluate the elastomeric behavior of GelMA-O5/rGO hydrogel. As shown in Fig. S4, the loading and unloading curves of the GelMA-O5/rGO hydrogel were nearly identical,

indicating good compressive resilience, which could withstand repeated cycles of stretching during cardiac beating [36].

Rheological tests were performed to characterize the viscoelastic properties of hydrogels (Fig. 2E). The storage modulus (G'), also known as elastic modulus, refers to the amount of energy stored due to elastic (reversible) deformation of a material when it is deformed, which reflects the elasticity of the material. With the increase of ODEX concentration, the G' of GelMA-O hydrogel increases, which indicates that the degree of Schiff based reaction between GelMA and ODEX increases, so

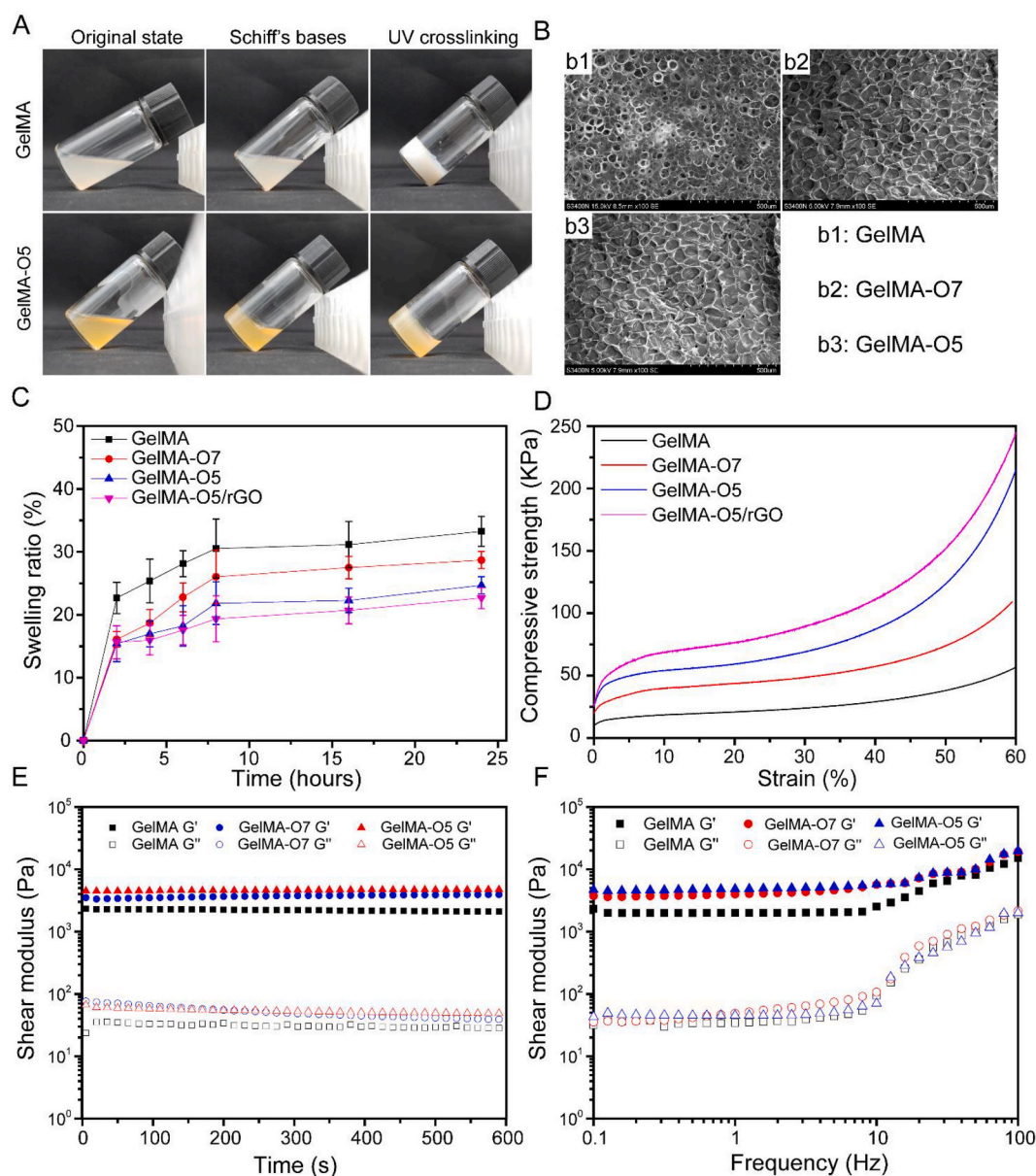


Fig. 2. (A) Photograph of the double-network hydrogel through a Schiff-based reaction (primary cross-linking network) and UV crosslinking (second cross-linking network). (B) SEM images of GelMA, GelMA-O7 and GelMA-O5 hydrogels. (C) The swelling ratio of hydrogels. (D) The compression modulus. The Compressive modulus was defined as the compressive strength at 60% strain. (E) The rheological properties. G' represents the storage modulus and G'' represents the loss modulus. (F) The hydrogel viscosity with frequency ranging from 0.1 to 100 Hz.

that the crosslinking density of hydrogel increases with the increase of ODEX content. Loss modulus (G''), also known as viscous modulus, refers to the amount of energy lost due to viscous deformation (irreversible) when the material is deformed, reflecting the viscosity of the material. As shown in Fig. 2F and G' is higher than G'' with the shear frequency from 0.1 to 100 rad/s, which indicating the hydrogels are stable and exhibit good mechanical properties. When beyond the linear frequency range, all hydrogels have a larger G' and increase commensurately with the increase of frequency. Meanwhile, the GelMA-O hydrogel showed improved viscoelasticity and dynamic property compared with GelMA hydrogel, which made it a potential candidate for myocardial tissue engineering.

3.3. Enzymatic degradation

Hydrogels should be bio-degradable for MI treatment. Thus, GelMA and GelMA-O5 hydrogels were measured through an *in vitro* degradation

experiment. The degradation rate of GelMA hydrogel without lysozyme were slower than that of hydrogel with lysozyme, and it takes about 7 days for hydrogel without lysozyme, but only about 5 days for hydrogel with lysozyme (Fig. 3A and Fig. 3B). The degradation of the hydrogels in pure PBS solution without lysozyme were due to hydrolysis. The degradation of the hydrogels in PBS solution with Lysozyme were due to a combination of enzymolysis and hydrolysis. Compared with pure GelMA hydrogel, the degradation rate of GelMA-O5 and GelMA-O5/rGO hydrogels is slower. The slow degradation rate is mainly due to the adding ODEX formed dual cross-linking network. The micromorphology of hydrogels could be directly observed by SEM (Fig. 3C and D). The holes in GelMA-O5 hydrogel are denser and more regular than pure GelMA hydrogel, which are consistent with the results of degradation rate. These results indicated that GelMA-O5 hydrogel with dual cross-linking network could efficiently enhance the stability of hydrogels under enzymatic hydrolysis condition, which was suitable for the treatment of MI, consistent with previous reports on material

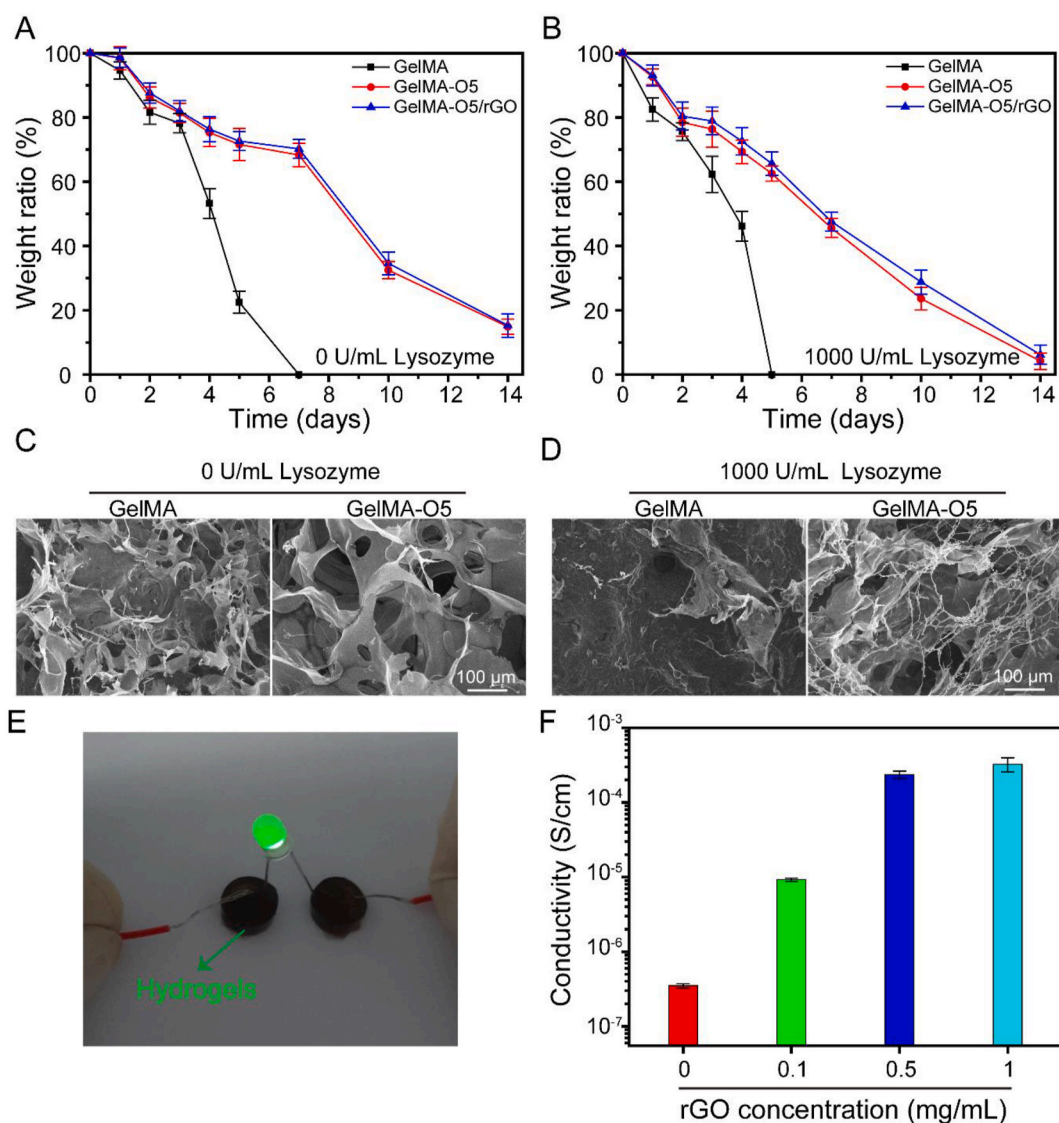


Fig. 3. The degradation of GelMA, GelMA-O5 and GelMA-O5/rGO hydrogels in pure PBS solution (A) and PBS solution containing 1000 U/mL Lysozyme (B) SEM images of the surface morphology of hydrogels at day 5, either in the presence (C) or absence (D) of 1000 U/mL Lysozyme. (E) GelMA-O5/rGO hydrogel was connected to a circuit and illuminated an LED. (F) Conductivity of the GelMA-O5/rGO hydrogel with different concentration of rGO.

degradation in MI.

3.4. Conductivity of hydrogels

The conductivity property of the GelMA-O5/rGO hydrogels was measured by four-probe method. As shown in Fig. 3E, the hydrogel can be incorporated into a circuit that lights up the light-emitting diode (LED), indicating that the hydrogel has good electrical conductivity. As shown in Fig. 3F, compared with GelMA-O5 hydrogels without GO, GelMA-O5/rGO hydrogels containing rGO show higher conductivity. Increasing the initial rGO concentration resulted in the increase of conductivity, indicating that the addition of rGO improves the electrical conductivity of the hydrogel system. Considering cell cytotoxicity of high concentration of rGO and the best conductivity, the hydrogel of 0.5 mg/mL rGO is chosen as the optimal group for the further study, and the electrical conductivity ($G = 2.36 \times 10^{-4}$ S/cm) of the hydrogel system is close to that of myocardial tissue ($G = 5 \times 10^{-5} - 1 \times 10^{-3}$ S/cm), which achieves the expected experimental goal [37]. Previous studies also shown that the conductivity (1.4×10^{-4} S/cm) of GO/CS scaffolds match in the range of reported conductivities for native cardiac tissue [38].

3.5. Biocompatible of cells in the hydrogel

In order to study the effect of hydrogels on UCMSCs survival and proliferation, we evaluated the biocompatibility of hydrogels *in vitro*. The UCMSCs were seeded on GelMA-O5 and GelMA-O5/rGO hydrogels, respectively. The adhesion and spreading of cells on hydrogels were observed by Live/Dead staining and CCK-8 method at days 1, 3 and 5. From the living/dead cell analysis, as shown in Fig. 4A, it can be seen that most UCMSCs were spread more evenly on all hydrogels at day 3. Meanwhile, there are almost no dead cells (red) on the surface of the hydrogel, indicating that all hydrogels display none cytotoxicity. In addition, the CCK-8 experiment indicated that the cell viability of GelMA-O5/rGO hydrogel group was comparable to GelMA-O5 hydrogel group at day 1 (Fig. 4B). Meanwhile, the cell survival rate on GelMA-O5/rGO hydrogel at day 5 was almost the same, and there was no significant difference compared with GelMA-O5 hydrogel group, indicating GO loaded GelMA-O5/rGO conducting hydrogel have excellent biocompatibility to be favorable for UCMSCs cells adhesion, spreading, and proliferation. As shown in Fig. 4C, the number of cells attached to the GelMA-O5/rGO hydrogel increased over time, and the cells attached to hydrogels began to grow and gather after 5 days of incubation. It was

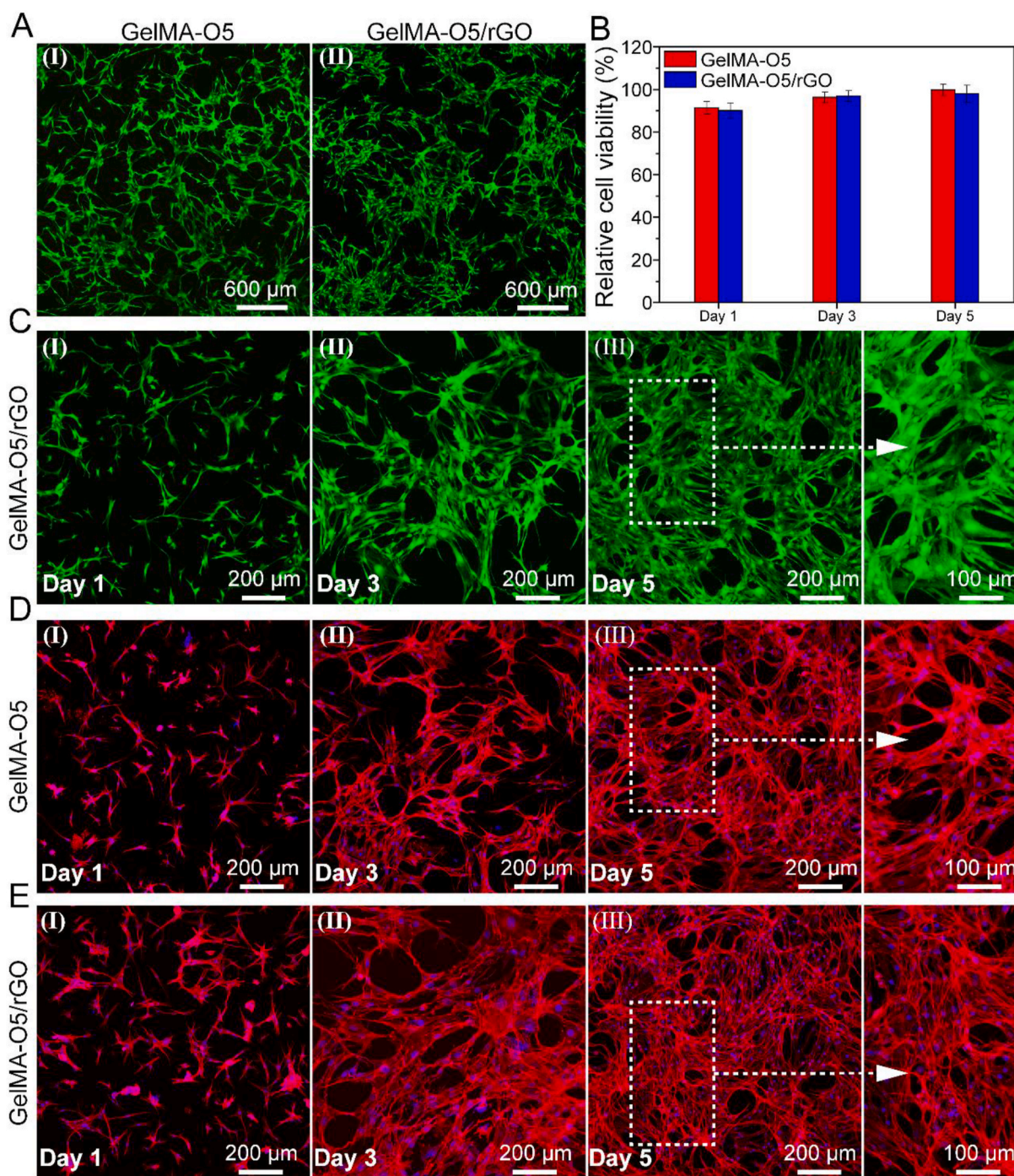


Fig. 4. (A) Live/dead staining images of UCMSCs cultured on GelMA-O5 (I) and GelMA-O5/rGO (II) hydrogels at day 3 (The green fluorescence represents living cells and the red fluorescence means dead cells). (B) Cell viability of UCMSCs cultured on hydrogels versus different culture times by CCK-8 assay. (C) Live/dead staining images of UCMSCs cultured on GelMA-O5/rGO hydrogels at day 1, day 3 and day 5. (D) Cell morphology of Umbilical cord mesenchymal stem cells (UCMSCs) in GelMA-O5 hydrogel. (E) Cell morphology of Umbilical cord mesenchymal stem cells (UCMSCs) in on GelMA-O5/rGO hydrogel. (For interpretation of the references to color in this figure legend, the reader is referred to the Web version of this article.)

mainly due to the fact that the dual network structure of GelMA-O5 is more conducive to cell adhesion and more biocompatible than GelMA network. As shown in Fig. 4D and E, most of the UCMSCs on the hydrogel can maintain the linear cell morphology, suggesting that the cell morphology is the same as that of the initial UCMSCs. All results showed that our hydrogel system could well maintain the biological activity of UCMSCs.

3.6. Cell encapsulation in hydrogel

The GelMA-O5/rGO hydrogel has good electrical activity and conductivity, which can promote cell differentiation. Thus, 3D cell culture experiments were performed to estimate the cell loading capacity of conducting Hydrogels. As shown in Fig. 5A, the staining photos of live/dead cells were corresponding to stem cells in conductive hydrogel at day 3. As shown in Fig. 5B, UCMSCs encapsulated in hydrogel have higher optical density (OD) value increased significantly from day 1 to

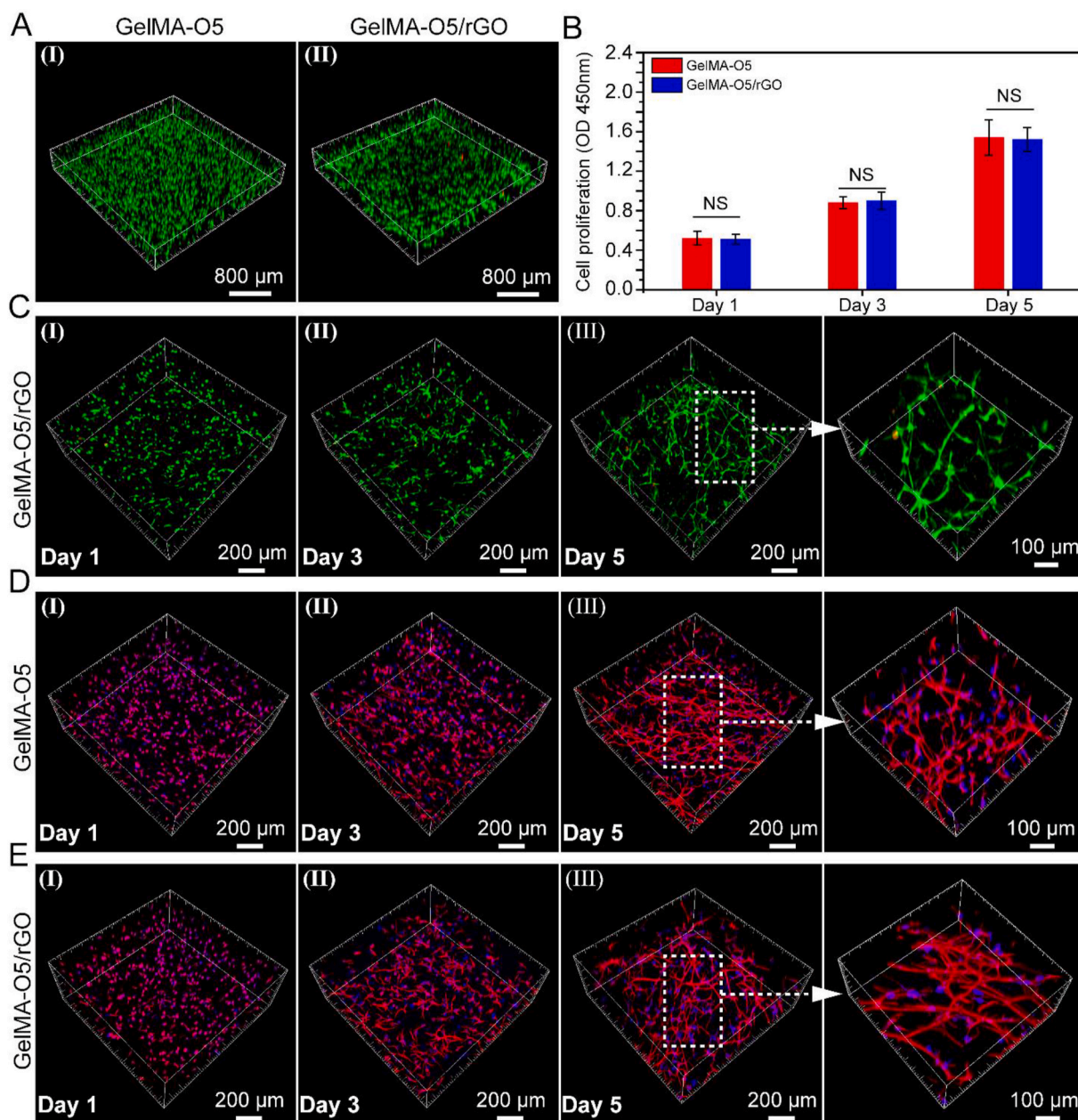


Fig. 5. (A) Representative 3D images of encapsulated cells inside GelMA-O5 (I) and GelMA-O5/rGO (II) hydrogels hydrogel network after 3 days of encapsulation (The green and red dots mean living and dead cells, respectively). (B) Proliferation of encapsulated UCMSCs inside GelMA-O5 and GelMA-O5/rGO hydrogels by CCK-8 assay. (C) Representative 3D images of encapsulated cells inside GelMA-O5/rGO hydrogel network after 1, 3 and 5 days of encapsulation. (D) Cell morphology of Umbilical cord mesenchymal stem cells (UCMSCs) in GelMA-O5 hydrogel. Phalloidin-TRITC and DAPI were used to stain actin filaments (F-actin) and cell nuclei, respectively. (E) Cell morphology of encapsulated UCMSCs inside GelMA-O5/rGO hydrogel. (For interpretation of the references to color in this figure legend, the reader is referred to the Web version of this article.)

day 5, which matches the results of 3D cell images. Because nutrients can efficiently diffuse through the hydrogel shell, cells can grow inside the hydrogel. Meanwhile, it also shows that the conductive hydrogel system has very low biotoxicity. As shown in Fig. 5C, we could obviously find that most of the UCMSCs maintained high cell viability (stained in green) after 24 h culture, and it could be found that only a few dead cells (stained in red) were observed in the images of live/dead staining within 5 days. It was noticeable that the morphology of UCMSCs grown on GelMA-O5/rGO hydrogel (Fig. 5E) was different from that on GelMA-O5 (Fig. 5D), which exhibited more elongation and thicker actin filaments. The degradability of GelMA-O5 and GelMA-O5/rGO hydrogels allows the neurite extension inside the 3D matrix.

3.7. Cell delivery properties of GelMA-O5/rGO

As the conductive hydrogel was expected to be used for cell delivery of heart repair, cell release in the heart after infarction was crucial for MI treatment and stem cell therapy, so the cell delivery ability of hydrogels was further studied. UCMSCs have been provided to have the ability to differentiate into myocardium, which is promising in improving cardiac function after infarction. Therefore, we selected UCMSCs to test the cell delivery capacity of hydrogels. The cells were tested for 6 days and the cell release was monitored every day. As shown in Fig. S5A, it was clear that most of the released UCMSCs were alive. As shown in Fig. S5B, the UCMSCs release curve showed a cumulative increasing monotonic trend, which implied that these hydrogels could provide a stable cell

supply to the cardiac tissue repair. Interestingly, the released UCMSCs inside GelMA-O5/rGO hydrogel network at day 6 showed linear cell morphology, which was the same as normal cultured stem cells (Fig. S5C), indicating that the cell function had been restored when the cell was released from the encapsulated GelMA-O5/rGO hydrogel. Because the pore diameter of the GelMA-O5 hydrogel is about 50 μm , and the diameter of stem cells is about 17 μm . Part of cell release is due to the pore of the hydrogel, and another part is attributable to the degradation of the hydrogel.

3.8. Effect of conducting hydrogels on *in vitro* cardiac differentiation of UCMSCs

Cardiac differentiation of stem cells is the most critical process for applications in cardiac tissue engineering [39,40]. The aforementioned results showed that GelMA-O5 hydrogel and GO-based GelMA-O5/rGO hydrogel exhibited almost same effect in terms of biocompatibility with UCMSCs. However, conductive hydrogels for GO have been provided to achieve better outcomes in the functionalization of stem cells, such as stem cell differentiation and maturation [41]. Cardiac Troponin I (cTnI) is a new specific cardiac biological marker, which is related to the maturation of myocardium and the regulation of muscle contraction [42]. The gap junction protein connexin 43 (Cx43) is mainly responsible for the electrical contraction coupling of myocardium and regulates the electrical signal transmission [43]. The arrangement of cell morphology implied the change of cell function. We mainly studied the functional differences of conducting hydrogels in stem cells through examining the expression of myocardial specific proteins and the ultrastructure.

Results in Fig. 6A showed the expression of cardiac-specific proteins in stem cells in GelMA-O5, GelMA-O5/rGO hydrogel and normal tissue culture plate (TCP). Immunofluorescence staining showed that cTnI and Cx43 were up-regulated in conductive hydrogel group compared with GelMA-O5 hydrogel group and TCP group. Compared with the expression of stem cells in GelMA-O5 hydrogel, more cTnI positive cardiomyocytes appeared in conductive hydrogel, and Cx43 protein was expressed at a higher level in cell membrane and between cells at day 7. In particular, GelMA-O5/rGO hydrogel showed strong expression of Cx43 at the plasma membrane between adjacent cells, which was not observed in TCPs. However, less expression of cTnI and Cx43 protein was found in TCPs. The reason of this phenomena is that rGO in GelMA-O5/rGO hydrogel with good electrochemical activity favors the exchange of chemicals and electrical signals between cells, which is conducive to cell differentiation. Meanwhile, the presented hydrogel exhibited moderate pore size, good mechanical properties, and appropriate water content for cell growth, which could increase the transport of oxygen and nutrients, and promote cell growth and differentiation [44].

Western blotting and PCR further demonstrated that the expression of cTnI and Cx43 protein of UCMSCs in the GelMA-O5/rGO conducting hydrogel increased significantly compared with GelMA-O5 hydrogel or TCPs at day 7 (Fig. 6B and C). In GelMA-O5/rGO gel, UCMSCs also detected higher expression of myocardial specific proteins than in TCPs (Fig. S6), which was consistent with the results of confocal microscopy. Prior studies demonstrated that the electric conduction of stem cells through conductive hydrogel could promote the differentiation of stem cells into myocardium, increased the connection in myocardium and

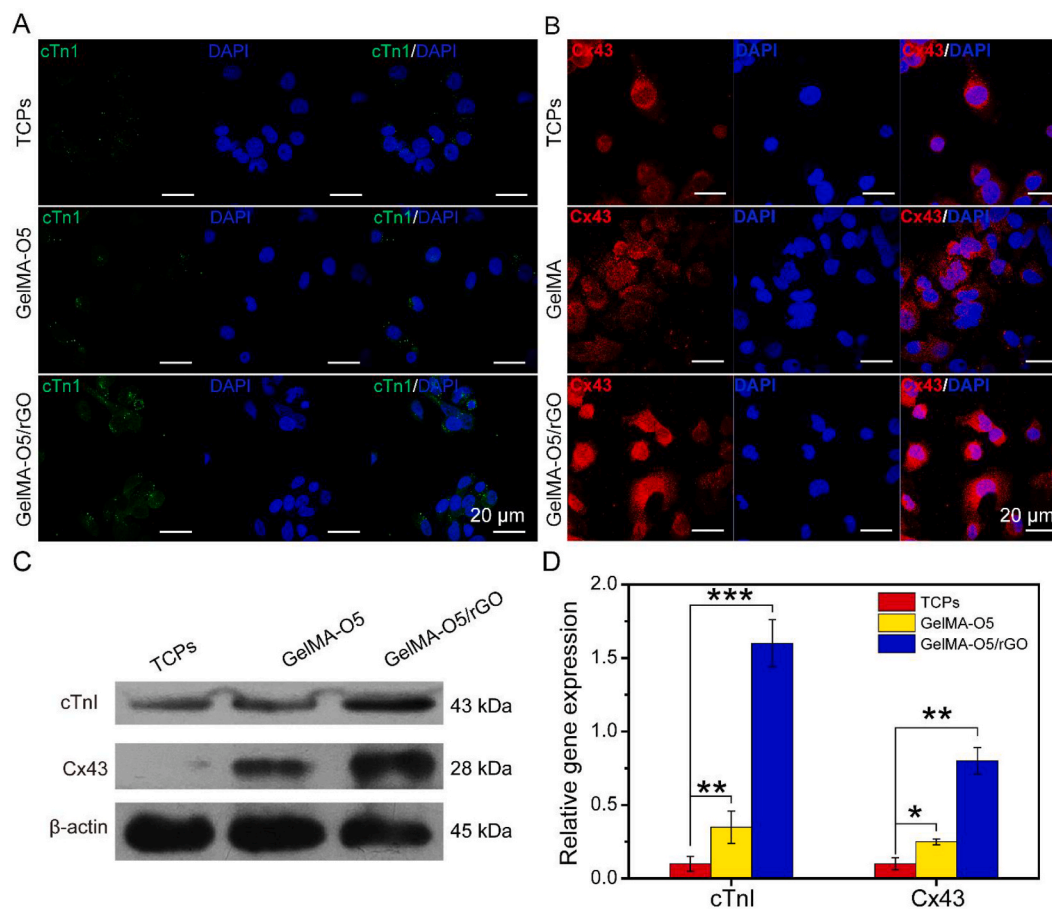


Fig. 6. (A) Expression of Cardiac Troponin I (cTnI) in UCMSCs on the TCPs, GelMA-O5, GelMA-O5/rGO hydrogel. (B) Expression of Connexin-43 (Cx43) in UCMSCs on the TCPs, GelMA-O5, GelMA-O5/rGO hydrogel. (C) Expression of cTnI and Cx43 in UCMSCs analyzed by western blotting. (D) RT-PCR quantitative analysis of cTnI and Cx43 in UCMSCs from three independent experiments for each group. (*) $P < 0.05$, (**) $P < 0.01$ and (***) $P < 0.001$.

functionalize stem cells cultured *in vitro* [45,46].

3.9. Tissue repair in infarcted area

As mentioned above, GelMA-O5 hydrogel showed an excellent performance for the growth of UCMSCs and their functionalization *in vitro*. We further investigated the role of GelMA-O5/rGO and GelMA-O5/rGO/UCMSCs hydrogels repair of infarcted cardiac muscle *in vivo*. As shown in Fig. 7A, Masson's trichrome staining showed that PBS group had a number of collagen zones occupying a large portion of the LV wall of the infarct site, which demonstrated the presence of widely spread scar tissue. However, fewer fibrous tissue was observed in GelMA-O5/rGO and GelMA-O5/rGO/UCMSCs hydrogel groups, which indicated that rGO exert a positive effect on cardiac repair. Prior study demonstrated that OPF/GO hydrogels could be microengineered to support microvascular networks *in vivo* and further improved the microenvironment of the infarcted region due to its appropriated conductivity and surface properties [47]. As shown in Fig. 7B, the infarct size of PBS, GelMA-O5, GelMA-O5/rGO and GelMA-O5/rGO/UCMSCs was $33.4 \pm 1.3\%$, $22.3 \pm 0.9\%$, $16.8 \pm 1.4\%$ and $7.1 \pm 1.0\%$, respectively. Compared with the PBS control group, the injection of GelMA-O5 hydrogel reduces the infarction area. Meanwhile, the addition of rGO and UCMSCs could significantly improve the infarction area of MI. Notably, GelMA-O5/rGO/UCMSCs group showed the smallest infarction area, which indicating that sustained release UCMSCs could better repair myocardium after infarction and reduce infarction. Lyu et al. reported that HA hydrogels encapsulating human mesenchymal stem cells (hMSCs) could promote the retention and survival rate of hMSCs in the infarction site, reduce infarction area and collagen deposition, and improve damaged myocardial function [48]. Consistent with above observation, LV wall thickness was significantly preserved (1.33 ± 0.28 mm vs 0.46 ± 0.1 mm) in the GelMA-O5/rGO/UCMSCs injected group compared to PBS injected group (Fig. 7C). As shown in Fig. S7, the GelMA-O5/rGO/UCMSCs group showed a large amount of red

fluorescence expression (PKH26-labeled UCMSCs) in heart tissue, while a low level of red fluorescence was observed in pure UCMSCs group. These results showed that hydrogel could provide continuous stem cells for heart tissue, and then exerts its biological functions. All results indicated that the structure of the infarcted heart was effectively improved after GelMA-O5/rGO/UCMSCs injection.

3.10. Functional improvement in infarcted area

To evaluate the contractile cardiac function, the rats at days 7, 14 and 28 post MI were subjected to echocardiogram analysis to assess cardiac function. As shown in Fig. 8A, the echocardiogram images were observed the deterioration in cardiac function of PBS group. However, GelMA-O5/rGO/UCMSCs and sham operation groups had similar baseline echocardiographic values. As shown in Fig. 8B and C, LV ejection fraction (EF) and fractional shortening (FS), two important indicators for blood pumping function, were improved in both GelMA-O5/rGO and GelMA-O5/rGO/UCMSCs groups compared to PBS-injected rats at days 28, which was due to that the hydrogels provided a mechanical support for the axial wall of the ventricle. Besides the sham operation group, EF and FS were significantly decreased in other groups at days 7 after injection, which indicated the occurrence of MI. Meanwhile, GelMA-O5/rGO/UCMSCs group showed higher EF ($82.8 \pm 1.7\%$ vs $40.5 \pm 2.2\%$) and FS ($53.2 \pm 1.5\%$ vs $20.7 \pm 1.0\%$) compared to PBS injected rats at days 28, which demonstrated a significant improvement of heart functions and efficient inhibition of ventricular remodeling. This was likely due to the longer survival time of UCMSCs in GelMA-O5/rGO hydrogel, which could improve cardiac mechanical function. As shown in Fig. S8A and Fig. S8B, both end-diastolic volume (EDV) and end-systolic volume (ESV) are significantly increased with the extension of time, which indicated that the heart undergoes the process of ventricular remodeling to ventricular dilation. Meanwhile, the values of EDV and ESV for the GelMA-O5/rGO/UCMSCs hydrogel group are lower than those of the GelMA-O5 and GelMA-O5/rGO hydrogel groups and are close to those of

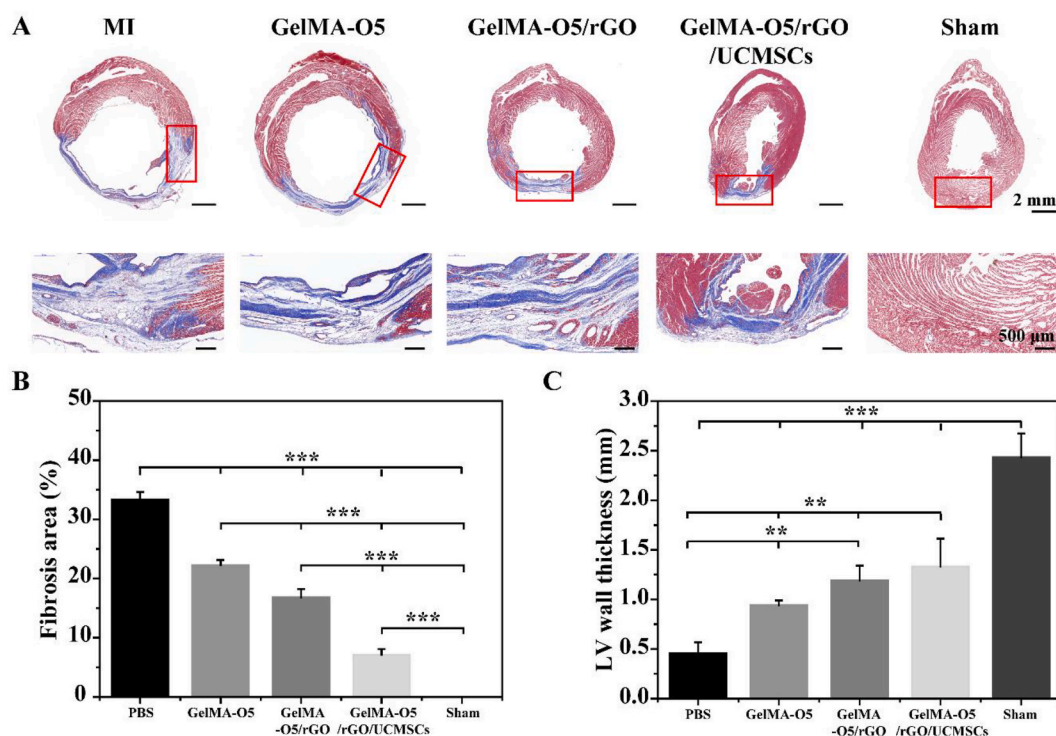


Fig. 7. (A) High-resolution images and locally enlarged views of Masson trichrome staining (Red, the muscle fibres; Green, collagen) in PBS, GelMA-O5, GelMA-O5/rGO and GelMA-O5/rGO/UCMSCs, sham operation groups after 4 weeks of injection. (B) Morphological analysis of infarct size of different groups. (C) Morphological analysis of wall thickness of different groups. (*) $P < 0.05$, (**) $P < 0.01$ and (***) $P < 0.001$. (For interpretation of the references to color in this figure legend, the reader is referred to the Web version of this article.)

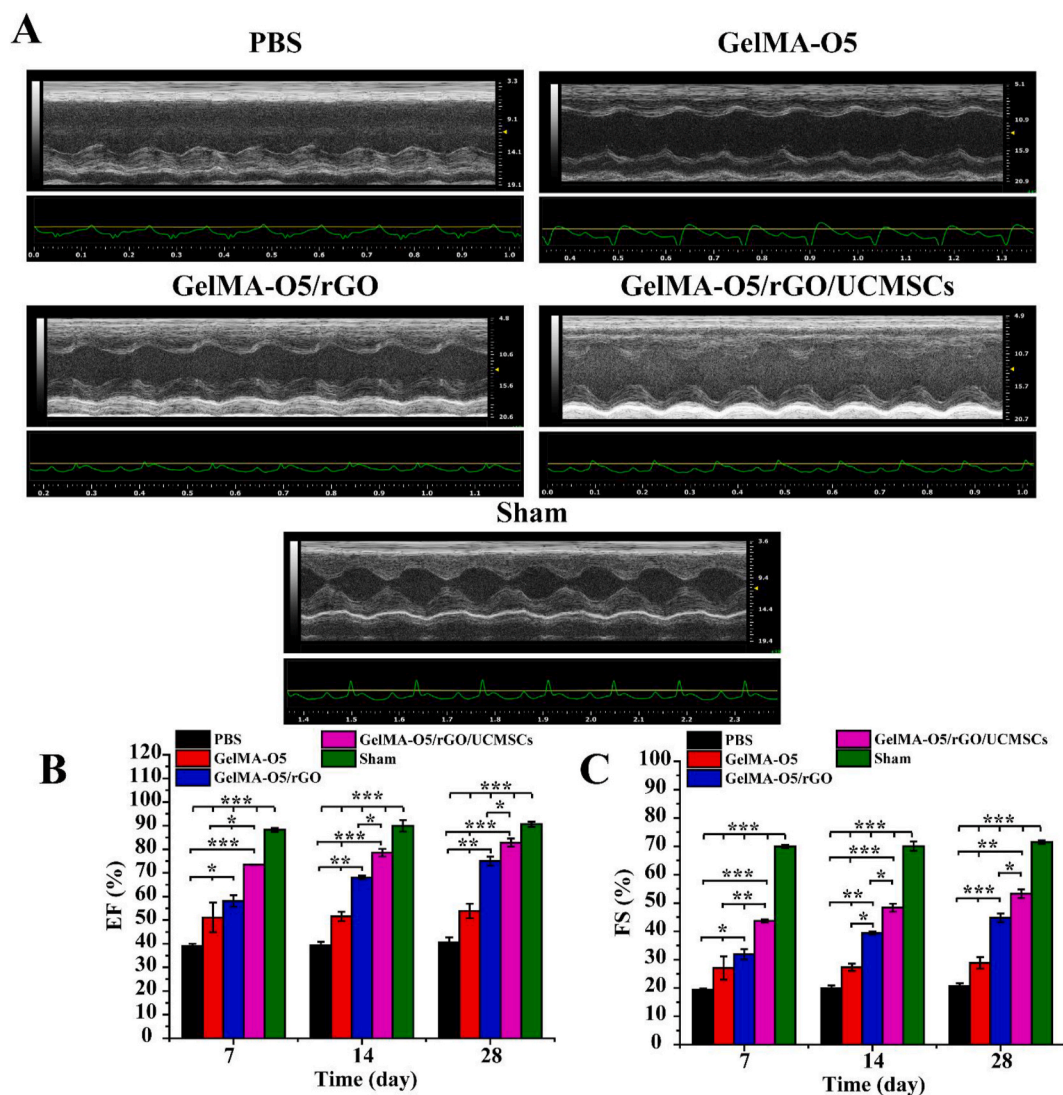


Fig. 8. (A) Representative echocardiograph images for PBS, GelMA-O5, GelMA-O5/rGO and GelMA-O5/rGO/UCMSCs, sham operation groups at 28 days post-injection. (B) Comparative analysis of LV ejection fraction (EF) at days 7, 14 and 28 post-injection. (C) Comparative analysis of fractional shortening (FS) at days 7, 14 and 28 post-injection. (*) $P < 0.05$, (**) $P < 0.01$ and (***) $P < 0.001$.

the sham operation group, which demonstrated that GelMA-O5/rGO/UCMSCs hydrogel can better preserved left ventricle geometry over 28 days after treatment. Prior studies have verified that an appropriate conductivity of the materials injected into the MI area could facilitate cardiac repair, which could improve the load-dependent ejection fraction/fractional shortening of heart function, and achieve more cardiac related marker expression and much higher spontaneous beating rates [49]. Yang et al. suggested that the hydrogels with a higher conductivity help the cardiac electrical signals to return to the initial state [50]. Previous studies showed that UCMSCs had stronger angiogenic potential and cellular activity, which is beneficial to enhance angiogenesis and cardiac function recovery in infarcted heart [10]. In summary, all results indicated GelMA-O5/rGO/UCMSCs hydrogel injection significantly promotes myocardial functional recovery after MI.

3.11. Immunofluorescence analysis

To further clarify the therapeutic mechanism of hydrogels for MI repair, immunofluorescence staining was carried out. Connexin-43 (Cx43, a gap junction protein) is responsible for electrical and metabolic coupling between cardiomyocytes and coordinates their contractility, which is essential in coordinated myocardial function [51,52].

Cardiac troponin I (cTnI, cardiac-specific markers) exists in the myofilaments of myocardial and striated muscle cells and participates in calcium-induced muscle contraction [53]. As shown in Fig. 9A and Fig. 9C, GelMA-O5/rGO/UCMSCs and sham operation group showed the strongest fluorescence signals of Cx43 and cTnI compared other groups. As shown in Fig. 9B and D, Cx43 and cTnI of the infarction area in PBS group decreased significantly compared with normal myocardium. However, GelMA-O5/rGO/UCMSCs group showed the highest expression of Cx43 and cTnI in MI area consisted with the sham operation group, which was likely due to that stem cells could promote Cx43 and cTnI expression and rGO could enhance the electrical activity in infarcted border zone.

MI includes cellular apoptosis and necrosis, and myocardial cell apoptosis is an important mode of MI. Caspase 3 (32 kDa) is a critical mediator of apoptosis, and the increased immunofluorescence of caspase-3 indicates the occurrence of apoptosis [54]. As shown in Fig. 9E, GelMA-O5/rGO/UCMSCs and sham operation group showed only minimal autofluorescence signal of caspase-3. As shown in Fig. 9F, the expression level of Caspase-3 was significantly greater in the PBS group compared with sham operation group, which indicated the excessive cardiomyocyte apoptosis after myocardial infarction. Meanwhile, the expression level of caspase-3 in all hydrogel groups was

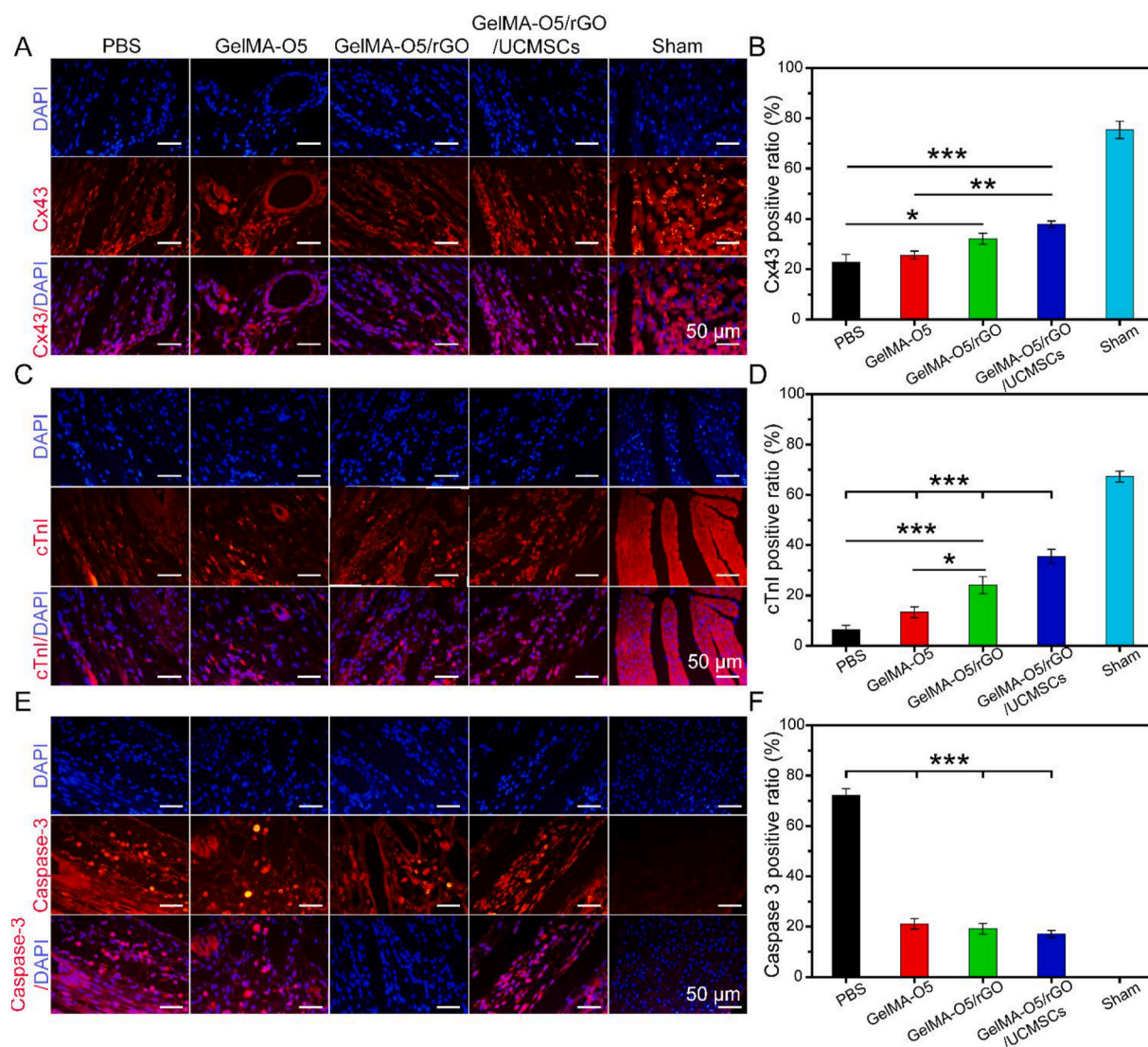


Fig. 9. (A) Representative images of Cx43 expression at peri-infarction area by IF staining. (B) Quantitative analysis of Cx43 expression. (C) Representative images of cTnI expression at peri-infarction area by IF staining. (D) Quantitative analysis of cTnI expression. (E) Representative images of caspase-3 expression at peri-infarction area by IF staining. (F) Quantitative analysis of caspase-3 expression. (*) $P < 0.05$, (**) $P < 0.01$ and (***) $P < 0.001$.

significantly reduced compared with the PBS group, which demonstrated that the mechanism of hydrogel in repairing myocardial infarction in rats is related to the reduction of apoptosis at the infarct border zone. Summary, UCMSCs repair infarcted myocardium through a variety of mechanisms, including direct differentiation, paracrine (promoting angiogenesis, anti-apoptosis, protection of myocardial ischemic injury), promoting nerve fiber regeneration, improving heart conduction and other possible mechanisms. The discovery of the new mechanism will help us to make better clinical application of stem cell therapy in the future.

4. Conclusions

Summarily, we have successfully designed and synthesized a conductive double network (GelMA-O5/rGO) hydrogels through combining the electrical conductivity of rGO with the biocompatibility of GelMA/ODEX hydrogels. These results showed that the swelling, mechanical and degradation properties of hydrogels could be regulated by adjusting the ratio of GelMA and ODEX. Meanwhile, by adjusting different rGO concentrations, the GelMA-O5/rGO hydrogel with 0.5

mg/mL rGO can match the range of electrical conductivity of native cardiac tissue. The results of CCK-8 test and live/dead stain test showed that the prepared hydrogel had good cytocompatibility, and the morphology test showed that UCMSCs could grow well on the surface of hydrogel. UCMSCs encapsulated in hydrogel had a good normal cell morphology, could continuously release cells, and improve the differentiation efficiency of stem cells through up-regulating the expression of cTnI and Cx43. Further *in vivo* experiments showed that GelMA-O5/rGO/UCMSCs could reduce infarct size and cardiac fibrosis in the infarct zone, increase ventricular ejection fraction, up-regulate the expression level of cTnI and Cx43, down-regulate the expression level of caspase-3, and finally improve heart function after MI. Collectively, the prepared injectable GelMA-O5/rGO/UCMSCs hydrogel opens a new option for treatment of MI.

CRediT authorship contribution statement

Shuoji Zhu: Conceptualization, Methodology, Software, Writing – review & editing. **Changjiang Yu:** Conceptualization, Methodology, Software. **Nanbo Liu:** Data curation, Writing – original draft. **Mingyi**

Zhao: Data curation, Writing – original draft. **Zerui Chen:** Visualization, Investigation. **Jian Liu:** Visualization, Investigation. **Ge Li:** Visualization, Investigation. **Huanlei Huang:** Supervision. **Huiming Guo:** Software, Validation. **Tucheng Sun:** Conceptualization, Methodology, Software. **Jimei Chen:** Data curation, Writing – original draft. **Jian Zhuang:** Data curation, Writing – original draft. **Ping Zhu:** Conceptualization, Methodology, Software, Writing – review & editing.

Declaration of competing interest

The authors declare no competing financial interest.

Acknowledgements

This work was supported by National Key Research and Development Program of China (2018YFA0108700, 2017YFA0105602), NSFC Projects of International Cooperation and Exchanges (81720108004), National Natural Science Foundation of China (81974019), the Research Team Project of Natural Science Foundation of Guangdong Province of China (2017A030312007), the key program of guangzhou science research plan (201904020047) and the Special Project of Dengfeng Program of Guangdong Provincial People's Hospital (DFJH201812, KJ012019119, KJ012019423).

Appendix A. Supplementary data

Supplementary data to this article can be found online at <https://doi.org/10.1016/j.bioactmat.2021.11.011>.

References

- [1] A. Majithia, D. Bhatt, A. Friedman, M. Miller, P. Steg, E. Brinton, T. Jacobson, S. Ketchum, R. Juliano, L. Jiao, R. Doyle, C. Granowitz, M. Budoff, R. Mason, J. Tardif, W. Boden, C. Ballantyne, Benefits of icosapent ethyl across the range of kidney function in patients with established cardiovascular disease or diabetes: reduce-it renal, *Circulation* 121 (2021) 055560.
- [2] S. Khan, Z. Javed, A. Lone, S. Dani, Z. Amin, S. Al-Kindi, S. Virani, G. Sharma, R. Blankstein, M. Blaha, M. Cainzos-Achirica, K. Nasir, Social vulnerability and premature cardiovascular mortality among US counties, 2014 to 2018, *Circulation* 144 (16) (2021) 1272–1279.
- [3] A. Patel, M. Salerno, R. Kwong, A. Singh, B. Heydari, C. Kramer, Stress cardiac magnetic resonance myocardial perfusion imaging: JACC review topic of the week, *J. Am. Coll. Cardiol.* 78 (16) (2021) 1655–1668.
- [4] M. Shilo, H. Oved, L. Wertheim, I. Gal, N. Noor, O. Green, E. Baruch, D. Shabat, A. Shapira, T. Dvir, Injectable nanocomposite implants reduce ROS accumulation and improve heart function after infarction, *Adv. Sci.* (2021), e2102919. Weinheim, Baden-Württemberg, Germany).
- [5] A. Ahmed, Y. Han, M. Al Rifai, T. Alnabalsi, F. Nabi, S. Chang, M. Cocker, C. Schwemmer, J. Ramirez-Giraldo, N. Kleiman, W. Zoghbi, J. Mahmarian, M. Al-Mallah, Prognostic Value of Computed Tomography-Derived Fractional Flow Reserve Comparison with Myocardial Perfusion Imaging, *JACC. Cardiovascular imaging*, 2021.
- [6] R. Williams, *Circulation research "in this issue" anthology*, *Circ. Res.* 122 (12) (2018) e92–e118.
- [7] R. Chen, C. Zhu, L. Xu, Y. Gu, S. Ren, H. Bai, Q. Zhou, X. Liu, S. Lu, X. Bi, W. Li, X. Jia, Z. Chen, An injectable peptide hydrogel with excellent self-healing ability to continuously release salvianolic acid B for myocardial infarction, *Biomaterials* 274 (2021) 120855.
- [8] M. Patil, S. Saheera, P. Dubey, A. Kahn-Krell, P. Govindappa, S. Singh, S. Tousif, Q. Zhang, H. Lal, J. Zhang, G. Qin, P. Krishnamurthy, Novel mechanisms of exosome-mediated phagocytosis of dead cells in injured heart, *Circ. Res.* 120 (2021) 317900.
- [9] R. Wu, W. Hu, H. Chen, Y. Wang, Q. Li, C. Xiao, L. Fan, Z. Zhong, X. Chen, K. Lv, S. Zhong, Y. Shi, J. Chen, W. Zhu, J. Zhang, X. Hu, J. Wang, A novel human long noncoding RNA SCDAL promotes angiogenesis through SNF5-mediated GDF6 expression, *Adv. Sci.* (2021), e2004629. Weinheim, Baden-Württemberg, Germany).
- [10] X. Ke, M. Li, X. Wang, J. Liang, X. Wang, S. Wu, M. Long, C. Hu, An injectable chitosan/dextran/ β -glycerophosphate hydrogel as cell delivery carrier for therapy of myocardial infarction, *Carbohydr. Polym.* 229 (2020) 115516.
- [11] N.G. Frangogiannis, J.C. Kovacic, Extracellular matrix in ischemic heart disease, Part 4/4: JACC focus seminar, *J. Am. Coll. Cardiol.* 75 (17) (2020) 2219–2235.
- [12] Y. Li, X. Chen, R. Jin, L. Chen, M. Dang, H. Cao, Y. Dong, B. Cai, G. Bai, J. G. Gooding, S. Liu, D. Zou, Z. Zhang, C. Yang, Injectable hydrogel with MSNs/microRNA-21-5p delivery enables both immuno modification and enhanced angiogenesis for myocardial infarction therapy in pigs, *Sci Adv* 7 (9) (2021).
- [13] S. Shaw, J.D. White, Asymmetric catalysis using chiral salen-metal complexes: recent advances, *Chem. Rev.* 119 (16) (2019) 9381–9426.
- [14] H. Li, J. Gao, Y. Shang, Y. Hua, M. Ye, Z. Yang, C. Ou, M. Chen, Folic acid derived hydrogel enhances the survival and promotes therapeutic efficacy of iPS cells for acute myocardial infarction, *ACS Appl. Mater. Interfaces* 10 (29) (2018) 24459–24468.
- [15] B. Qian, Q. Yang, M. Wang, S. Huang, C. Jiang, H. Shi, Q. Long, M. Zhou, Q. Zhao, X. Ye, Encapsulation of lyophilized platelet-rich fibrin in alginate-hyaluronic acid hydrogel as a novel vascularized substitution for myocardial infarction, *Bioactive. Mater.* 7 (2022) 401–411.
- [16] X. Ke, M. Li, X. Wang, J. Liang, X. Wang, S. Wu, M. Long, C. Hu, An injectable chitosan/dextran/ β -glycerophosphate hydrogel as cell delivery carrier for therapy of myocardial infarction, *Carbohydr. Polym.* 229 (2020) 115516.
- [17] L. Ptaszek, R. Portillo Lara, E. Shirzaei Sani, C. Xiao, J. Roh, X. Yu, P. Ledesma, C. Hsiang Yu, N. Annabi, J. Ruskin, Gelatin methacryloyl bioadhesive improves survival and reduces scar burden in a mouse model of myocardial infarction, *J. Am. Heart Assoc.* 9 (11) (2020), e014199.
- [18] J. Ding, Y. Yao, J. Li, Y. Duan, J. Nakkala, X. Feng, W. Cao, Y. Wang, L. Hong, L. Shen, Z. Mao, Y. Zhu, C. Gao, A reactive oxygen species scavenging and O generating injectable hydrogel for myocardial infarction treatment in vivo, *Small* 16 (48) (2020), e2005038.
- [19] P. Contessotto, D. Orbanic, M. Da Costa, C. Jin, P. Owens, S. Chantepie, C. Chinello, J. Newell, F. Magni, D. Papy-Garcia, N. Karlsson, M. Kilcoyne, P. Dockery, J. Rodríguez-Cabello, A. Pandit, Elastin-like recombinamers-based hydrogel modulates post-ischemic remodeling in a non-transmural myocardial infarction in sheep, *Sci. Transl. Med.* 13 (581) (2021).
- [20] Z. Zhao, G. Li, H. Ruan, K. Chen, Z. Cai, G. Lu, R. Li, L. Deng, M. Cai, W. Cui, via Capturing magnesium ions microfluidic hydrogel microspheres for promoting cancellous bone regeneration, *ACS Nano* 15 (2021) 13041–13054.
- [21] Y. Lee, O. Jeon, S. Lee, A. Ding, D. Wells, E. Alsberg, Induction of 4D spatiotemporal geometric transformations in high cell density tissues via shape changing hydrogels, *Adv. Funct. Mater.* 31 (24) (2021).
- [22] F. Gao, Z. Xu, Q. Liang, H. Li, L. Peng, M. Wu, X. Zhao, X. Cui, C. Ruan, W. Liu, Osteochondral regeneration with 3D-printed biodegradable high-strength supramolecular polymer reinforced-gelatin hydrogel scaffolds, *Adv. Sci.* 6 (15) (2019) 1900867.
- [23] X. Song, X. Wang, J. Zhang, S. Shen, W. Yin, G. Ye, L. Wang, H. Hou, X. Qiu, A tunable self-healing ionic hydrogel with microscopic homogeneous conductivity as a cardiac patch for myocardial infarction repair, *Biomaterials* 273 (2021) 120811.
- [24] J. Zheng, J. Zhang, D. Kong, Y. Song, S. Zhao, W. Qi, Y. Li, M. Zhang, X. Huang, Quantification of the CM-Dil-labeled human umbilical cord mesenchymal stem cells migrated to the dual injured uterus in SD rat, *Stem Cell Res. Ther.* 11 (1) (2020) 280.
- [25] C. Song, X. Zhang, L. Wang, F. Wen, K. Xu, W. Xiong, C. Li, B. Li, Q. Wang, M. Xing, X. Qiu, An injectable conductive three-dimensional elastic network by tangled surgical-suture spring for heart repair, *ACS Nano* 13 (12) (2019) 14122–14137.
- [26] R. Dong, P.X. Ma, B. Guo, Conductive biomaterials for muscle tissue engineering, *Biomaterials* 229 (2020) 119584.
- [27] C.N. Yeh, H. Huang, A.T.O. Lim, R.H. Jhang, C.H. Chen, J. Huang, Binder-free graphene oxide doughs, *Nat. Commun.* 10 (1) (2019) 422.
- [28] S. Shin, C. Zihlmann, M. Akbari, P. Assawas, L. Cheung, K. Zhang, V. Manoharan, Y. Zhang, M. Yükksekaya, K. Wan, M. Nikkha, M. Dokmeci, X. Tang, A. Khademhosseini, Reduced graphene oxide-GelMA hybrid hydrogels as scaffolds for cardiac tissue engineering, *Small* 12 (27) (2016) 3677–3689.
- [29] B. Kong, Y. Chen, R. Liu, X. Liu, C. Liu, Z. Shao, L. Xiong, X. Liu, W. Sun, S. Mi, Fiber reinforced GelMA hydrogel to induce the regeneration of corneal stroma, *Nat. Commun.* 11 (1) (2020) 1435.
- [30] Z. Wei, S. Gerecht, A self-healing hydrogel as an injectable instructive carrier for cellular morphogenesis, *Biomaterials* 185 (2018) 86–96.
- [31] J. Yang, Y. Yang, N. Kawazoe, G. Chen, Encapsulation of individual living cells with enzyme responsive polymer nanoshell, *Biomaterials* 197 (2019) 317–326.
- [32] S. Huang, H. Liu, K. Liao, Q. Hu, R. Guo, K. Deng, Functionalized GO nanovehicles with nitric oxide release and photothermal activity-based hydrogels for bacteria-infected wound healing, *ACS Appl. Mater. Interfaces* 12 (26) (2020) 28952–28964.
- [33] W. Cui, M. Li, J. Liu, B. Wang, C. Zhang, L. Jiang, Q. Cheng, A strong integrated strength and toughness artificial nacre based on dopamine cross-linked graphene oxide, *ACS Nano* 8 (9) (2014) 9511–9517.
- [34] K. Yue, G. Trujillo-de Santiago, M.M. Alvarez, A. Tamayol, N. Annabi, A. Khademhosseini, Synthesis, properties, and biomedical applications of gelatin methacryloyl (GelMA) hydrogels, *Biomaterials* 73 (2015) 254–271.
- [35] H. Cui, C. Liu, T. Esworthy, Y. Huang, Z.X. Yu, X. Zhou, H. San, S.J. Lee, S.Y. Hann, M. Boehm, M. Mohiuddin, J.P. Fisher, L.G. Zhang, 4D physiologically adaptable cardiac patch: a 4-month in vivo study for the treatment of myocardial infarction, *Sci Adv* 6 (26) (2020), eabb5067.
- [36] B.W. Walker, R.P. Lara, C.H. Yu, E.S. Sani, W. Kimball, S. Joyce, N. Annabi, Engineering a naturally-derived adhesive and conductive cardio patch, *Biomaterials* 207 (2019) 89–101.
- [37] X. Yi, J. He, X. Wang, Y. Zhang, G. Tan, Z. Zhou, J. Chen, D. Chen, R. Wang, W. Tian, P. Yu, L. Zhou, C. Ning, Tunable mechanical, antibacterial, and cytocompatible hydrogels based on a functionalized dual network of metal coordination bonds and covalent crosslinking, *ACS Appl. Mater. Interfaces* 10 (7) (2018) 6190–6198.
- [38] L. Jiang, D. Chen, Z. Wang, Z. Zhang, Y. Xia, H. Xue, Y. Liu, Preparation of an electrically conductive graphene oxide/chitosan scaffold for cardiac tissue engineering, *Appl. Biochem. Biotechnol.* 188 (4) (2019) 952–964.

- [39] H. Cha, Ö. Uyan, Y. Kai, T. Liu, Q. Zhu, Z. Tothova, G. Botten, J. Xu, G. Yuan, J. Dekker, S. Orkin, Inner nuclear protein Matrin-3 coordinates cell differentiation by stabilizing chromatin architecture, *Nat. Commun.* 12 (1) (2021) 6241.
- [40] J. Tan, J. Guyette, K. Miki, L. Xiao, G. Kaur, T. Wu, L. Zhu, K. Hansen, K. Ling, D. Milan, H. Ott, Human iPSC-derived pre-epicardial cells direct cardiomyocyte aggregation expansion and organization in vitro, *Nat. Commun.* 12 (1) (2021) 4997.
- [41] J. Yang, K. Hsieh, P. Kumar, S. Cheng, Y. Lin, Y. Shen, G. Chen, Enhanced osteogenic differentiation of stem cells on phase-engineered graphene oxide, *ACS Appl. Mater. Interfaces* 10 (15) (2018) 12497–12503.
- [42] Z. Li, Z. Fan, Y. Xu, W. Lo, X. Wang, H. Niu, X. Li, X. Xie, M. Khan, J. Guan, pH-sensitive and thermosensitive hydrogels as stem-cell carriers for cardiac therapy, *ACS Appl. Mater. Interfaces* 8 (17) (2016) 10752–10760.
- [43] M. Jarafiz-Rodríguez, M.D. Taberero, M. González-Tablas, A. Otero, A. Orfao, J. M. Medina, A. Taberero, A short region of Connexin43 reduces human glioma stem cell migration, invasion, and survival through src, PTEN, and FAK, *Stem Cell Rep.* 9 (2) (2017) 451–463.
- [44] A. Navaei, D. Truong, J. Heffernan, J. Cutts, D. Brafman, R. Sirianni, B. Vernon, M. Nikkiah, PNIPAAm-based biohybrid injectable hydrogel for cardiac tissue engineering, *Acta Biomater.* 32 (2016) 10–23.
- [45] G. Basara, M. Saeidi-Javash, X. Ren, G. Bahcecioglu, B. Wyatt, B. Anasori, Y. Zhang, P. Zorlutuna, Electrically conductive 3D printed TiCT MXene-PEG composite constructs for cardiac tissue engineering, *Acta Biomater.* (2020), <https://doi.org/10.1016/j.actbio.2020.12.033>.
- [46] R. Bao, B. Tan, S. Liang, N. Zhang, W. Wang, W. Liu, A π - π conjugation-containing soft and conductive injectable polymer hydrogel highly efficiently rebuilds cardiac function after myocardial infarction, *Biomaterials* 122 (2017) 63–71.
- [47] J. Zhou, X. Yang, W. Liu, C. Wang, Y. Shen, F. Zhang, H. Zhu, H. Sun, J. Chen, J. Lam, A. Mikos, C. Wang, Injectable OPF/graphene oxide hydrogels provide mechanical support and enhance cell electrical signaling after implantation into myocardial infarct, *Theranostics* 8 (12) (2018) 3317–3330.
- [48] Y. Lyu, J. Xie, Y. Liu, M. Xiao, Y. Li, J. Yang, J. Yang, W. Liu, Injectable hyaluronic acid hydrogel loaded with functionalized human mesenchymal stem cell aggregates for repairing infarcted myocardium, *ACS Biomater. Sci. Eng.* 6 (12) (2020) 6926–6937.
- [49] J. Zhou, X. Yang, W. Liu, C. Wang, Y. Shen, F. Zhang, H. Zhu, H. Sun, J. Chen, J. Lam, A.G. Mikos, C. Wang, Injectable OPF/graphene oxide hydrogels provide mechanical support and enhance cell electrical signaling after implantation into myocardial infarct, *Theranostics* 8 (12) (2018) 3317–3330.
- [50] B. Yang, F. Yao, T. Hao, W. Fang, L. Ye, Y. Zhang, Y. Wang, J. Li, C. Wang, Development of electrically conductive double-network hydrogels via one-step facile strategy for cardiac tissue engineering, *Adv Healthc Mater* 5 (4) (2016) 474–488.
- [51] R. Bohuslavova, R. Cerychova, F. Papousek, V. Olejnickova, M. Bartos, A. Görlach, F. Kolar, D. Sedmera, G. Semenza, G. Pavlinkova, HIF-1 α is required for development of the sympathetic nervous system, *Proc. Natl. Acad. Sci. U.S.A.* 116 (27) (2019) 13414–13423.
- [52] C. Tu, R. Mezynski, J. Wu, Improving the engraftment and integration of cell transplantation for cardiac regeneration, *Cardiovasc. Res.* 116 (3) (2020) 473–475.
- [53] K. Eggers, B. Lagerqvist, P. Venge, L. Wallentin, B. Lindahl, Persistent cardiac troponin I elevation in stabilized patients after an episode of acute coronary syndrome predicts long-term mortality, *Circulation* 116 (17) (2007) 1907–1914.
- [54] Y. Wang, S.Y. Li, S. Shen, J. Wang, Protecting neurons from cerebral ischemia/reperfusion injury via nanoparticle-mediated delivery of an siRNA to inhibit microglial neurotoxicity, *Biomaterials* 161 (2018) 95–105.